

Statistical study of release time and its energy dependence of in-situ energetic electrons in impulsive solar flares

Xiangyu Wu^{1,2}, Gang Li², Lulu Zhao³, Frederic Effenberger^{4,5}, Linghua Wang⁶, Shuo Yao¹

¹School of Geophysics and Information Technology, China University of Geosciences, Beijing, China

²Department of Space Sciences, University of Alabama in Huntsville, USA

³Department of Climate and Space Sciences and Engineering (CLaSP), University of Michigan, Ann Arbor, MI 48109, USA

⁴Institut für Theoretische Physik, IV, Ruhr-Universität Bochum, 44780 Bochum, Germany

⁵Bay Area Environmental Research Institute, NASA Research Park, Moffett Field, CA, USA

⁶School of Earth and Space Sciences, Peking University, Beijing, 100871, People's Republic of China

Key Points:

- delay of the release of in-situ electrons from hard X-ray generating electrons in impulsive SEP events is examined for 29 events
- clear delays are seen in all events and in most events the delay is energy dependent
- the delay shows no energy dependence in fewer than 20% events and the traditional VDA method only applies in these events

Corresponding author: Gang Li, gangli.uahuntsville@gmail.com

This is the author manuscript accepted for publication and has undergone full peer review but has not been through the copyediting, typesetting, pagination and proofreading process, which may lead to differences between this version and the [Version of Record](#). Please cite this article as [doi: 10.1029/2022JA030939](https://doi.org/10.1029/2022JA030939).

This article is protected by copyright. All rights reserved.

Abstract

Using the Fraction Velocity Dispersion Analysis (FVDA) method, it has been shown recently that in two impulsive solar energetic electron (SEE) events, the release times of near-relativistic electrons at the Sun for outward propagating electrons are energy dependent and are delayed compared to those of the downward propagating electrons. In this work, we perform a statistical study of the release time and its energy dependence of near-relativistic electrons in impulsive SEE events. We use in-situ observations from the Wind spacecraft and remote hard X-ray observations from the RHESSI and/or Fermi spacecraft. The difference of the release times between outward electrons and downward electrons for 29 events are obtained. In all events the release of the outward propagating electrons are delayed from those precipitating downward. In 26 of the 29 events, the release times of outward propagating electrons also show clear energy dependence. In 15 of these 26 events, in-situ electron data from more than 5 energy channels were available. The delay time as a function of energy for 9 of these can be fitted by a form proposed by [G. Li et al. \(2021\)](#). The implication of this energy dependent release on the MHD turbulence property at the electron acceleration site is discussed.

1 Introduction

While solar flares are generally regarded as a major site that accelerates solar energetic particles (SEPs), the underlying acceleration mechanism is still under debate. In the standard flare model (CSHKP model) ([Carmichael, 1964](#); [Hirayama, 1974](#); [Kopp & Pneuman, 1976](#); [Sturrock, 1966](#)), ions and electrons are accelerated by the released magnetic energy during magnetic reconnection. Electrons precipitating to the solar surface generate Hard X-ray (HXR), and due to the occurrence of reconnection between closed field lines, electrons cannot escape. An interchange reconnection, proposed by [Heyvaerts et al. \(1977\)](#), refined by [Vrnak et al. \(2003\)](#) and [Krucker et al. \(2007\)](#), introduces a scenario where magnetic reconnection occurs between closed and open field lines, leading to the escape of flare-accelerated energetic particles into the solar wind. In the work of [Masson et al. \(2013\)](#), an intrinsic interchange reconnection is identified to account for the escape of accelerated energetic particles into the heliosphere.

If electrons are accelerated at an interchange reconnection site, the accelerated electrons can propagate both outward and downward so that the outward propagating electrons and the HXR-generating electrons are released at the same time, i.e. simultaneous release of electrons. Recently, [G. Li, Zhao, et al. \(2020\)](#); [G. Li et al. \(2021\)](#) tested this idea of simultaneous release in two impulsive energetic electron events, the 2001-04-25 event and the 2016-07-23 event. In both events, in-situ electrons were observed by the 3D Plasma and Energetic Particle (3DP) instruments on Wind. By applying the Fractional Velocity Dispersion Analysis (FVDA) method [Zhao et al. \(2019\)](#), they obtain the release times of in-situ electrons at the Sun. They also used hard X-rays observations to obtain proxies of the release times of downward precipitating energetic electrons. They found that in both events the outward propagating electrons are released later than the HXR-generating electrons, indicating that these two electron populations are likely of two different populations and the simple interchange reconnection scenario can not explain both events.

The timing study of ([G. Li, Zhao, et al., 2020](#); [G. Li et al., 2021](#)) support earlier results by [Haggerty and Roelof \(2002\)](#) and [Haggerty et al. \(2003\)](#) who used the Advanced Composition Explorer (ACE) observations compared to the inferred solar release time of in-situ energetic electrons. For over 70 events, [Haggerty and Roelof \(2002\)](#) compared the release time of in-situ near-relativistic electrons (using highest-energy channel available and assuming a 1.2 au nominal path length) with HXR start time and found a 10 \sim 20 minute delay. In addition to a delay between the outward propagating electrons and the downward propagating electrons, the release of outward propagating electrons

71 can be also energy-dependent. In the work of [L. Wang et al. \(2006, 2016\)](#), a delay be-
72 tween the injection of high-energy electrons and low-energy electrons in SEP events was
73 found. Such a delay was also noted earlier by [Krucker et al. \(1999\)](#), [Haggerty and Roelof](#)
74 [\(2002\)](#), [Simnett et al. \(2002\)](#), and [Klein et al. \(2005\)](#). The delay can be a natural con-
75 sequence of the underlying acceleration process: it takes longer time to accelerate par-
76 ticles to higher energies, consequently a later release. One useful observation that can
77 better help understanding this delay is type III radio bursts. In a statistical study of 79
78 solar electron events, [Cane \(2003\)](#) examined possible delay of in-situ electrons from the
79 accompanying type III radio bursts. Using the electron release times determined by [Haggerty](#)
80 [and Roelof \(2002\)](#), [Cane \(2003\)](#) found a correlation between this delay and solar wind
81 density (See Figure 4 of [Cane \(2003\)](#)). Events with longer delays tend to have larger so-
82 lar wind density. [Cane \(2003\)](#) suggested that interplanetary conditions such as pitch an-
83 gle scattering may be responsible for such a delay and argued that type III generating
84 electrons and in-situ electrons could be of the same population. However, the uncertainty
85 of this correlation appears to be large. Furthermore, the electron release times were de-
86 termined using the traditional VDA method for selected electron energy bins ([Haggerty](#)
87 [& Roelof, 2002](#)), which is less accurate compared to the FVDA method employed here.
88 In this work, we also include type III radio bursts. As will be shown, there is no clear
89 evidence of a delay between the release time of type III radio bursts and in-situ electrons.
90 Nevertheless, the work of [Cane \(2003\)](#) illustrated the importance of the propagation ef-
91 fect in examining electron events.

92 If indeed the delay of release is due to acceleration (other processes such as trap-
93 ping may also lead to delayed releases), then the energy dependence of the delay offers
94 an opportunity to examine the underlying acceleration process. In the 2016-07-23 event,
95 [G. Li et al. \(2021\)](#) examined the energy dependence of the release times and found that
96 the delay can be fitted by a power-law form. From the power law index of the fitting,
97 they inferred the MHD turbulence power spectrum at the acceleration site.

98 The work of [G. Li et al. \(2021\)](#) calls for a statistical study of the release time and
99 its energy dependence of energetic electrons in impulsive events. Such a statistical study
100 requires an accurate determination of the release times of energetic electrons at the Sun.
101 This can be achieved by the FVDA method developed by [Zhao et al. \(2019\)](#). In this work,
102 we use the FVDA method to examine the energy dependence of the release times of en-
103 ergetic electrons in 29 impulsive events. In all events, we find that the outward propa-
104 gating electrons are released later than those HXR-generating electrons. The release of
105 the outward propagating electrons shows clear energy dependence for 26 events and shows
106 no/weak energy dependence in three events. In 15 events in-situ electron observation for
107 more than 5 energy channels are obtained. For these events we further apply the anal-
108 ysis in [G. Li et al. \(2021\)](#) to fit the energy release time delay by a power law of the elec-
109 tron momentum. For 9 out of 15 events, reasonable fittings were obtained and the fit-
110 ting results are shown in Table 2 and Figure 5. The implication of the fitted power law
111 index on the flare turbulence spectrum is discussed.

112 2 Event Selection and the FVDA method

113 In-situ energetic electrons are measured by the 3D Plasma and Energetic Particle
114 (3DP) instrument on board the WIND spacecraft ([Lin et al., 1995](#)). The silicon semi-
115 conductor telescopes (SST) in the 3DP instrument provide three-dimensional measure-
116 ments of electrons distributions from ~ 25 keV to ~ 400 keV with energy resolution of ~ 7
117 keV FWHM and angular resolution of $22^\circ.5 \times 36^\circ$. Energetic electron observations are
118 combined with the detection of type III radio bursts that are captured by WAVES in-
119 strument on board the WIND spacecraft and/or SWAVES instrument on Solar Terres-
120 trial Relations Observatory (STEREO). Hard X-rays are observed by either the Ramaty
121 High Energy Solar Spectroscopic Imager (RHESSI), or the Fermi/GBM. RHESSI was
122 launched in February 2002 and it detects solar photons from 3 keV to 17 MeV ([Smith](#)

123 [et al., 2003](#)). Fermi was launched in June 2008, and the GBM instrument consists of 12
 124 Sodium Iodide (NaI) detectors covering the energy range between 8 to 1,000 keV and
 125 two Bismuth Germanate (BGO) detectors covering the energies of 200 keV to 40 MeV
 126 ([Meegan et al., 2009](#)). Both RHESSI and Fermi/GBM have high time and energy res-
 127 olution and are capable of determining the release time of HXR-generating electrons.

128 For our study, a RHESSI hard X-ray event list and an in-situ electron event list
 129 are used. The RHESSI flare list is based on the flare database maintained by the RHESSI
 130 team at [https://hesperia.gsfc.nasa.gov/rhessi3/data-access/rhessi-data/flare-](https://hesperia.gsfc.nasa.gov/rhessi3/data-access/rhessi-data/flare-list/index.html)
 131 [-list/index.html](https://hesperia.gsfc.nasa.gov/rhessi3/data-access/rhessi-data/flare-list/index.html). Only flares with a valid GOES classification are considered. This
 132 list is then correlated with in-situ electron observations by Wind ([L. Wang et al., 2012](#);
 133 [W. Wang et al., 2021](#)). An event is identified as a potential event if the hard X-ray peak
 134 time from the RHESSI observation and the in-situ onset time of energetic electrons from
 135 the Wind observation are within 20 minutes. We then select events for our study with
 136 the following criteria:

- 137 (1) in-situ observation of the event by Wind must have fast rising phase (onset and
 138 peak of the event must be within an hour) and the average pre-event background
 139 $+3\sigma$ should be lower than one fourth of the peak flux;
- 140 (2) the time intensity profiles of in-situ electrons are detected by at least 4 energy chan-
 141 nels of WIND/3DP with similar shapes, in the energy range of 27-310 keV;
- 142 (3) events need to be observed by either RHESSI or Fermi in at least one of the two
 143 energy channels: 25 keV or 50 keV. For large solar flares with complicated mag-
 144 netic field structures, hard X-ray time profiles often show multiple peaks during
 145 the event. We take the first episode as the HXR observation of the event.

146 With these criteria, a total of 29 events are identified. For all these events, we do not
 147 use omni-direction electron intensity data, but only use electron data from sectors that
 148 align with the nominal Parker field direction and are sunward facing. This is to ensure
 149 that our analysis is not contaminated by possible preceding events in which inward prop-
 150 agating electrons may be detected during our events. Indeed, previous studies have shown
 151 evidence that energetic electrons can propagate toward the Sun due to the reflection be-
 152 yond 1 au or near the Sun in a magnetic loop ([Anderson et al., 1995](#); [Tan et al., 2009](#),
 153 [2012](#); [G. Li, Wu, et al., 2020](#)). Next, we apply the FVDA method ([Zhao et al., 2019](#); [G. Li,](#)
 154 [Zhao, et al., 2020](#); [G. Li et al., 2021](#)) to compute the path length L and the release times
 155 T_r of outward-propagating electrons. In the original VDA method ([Lin, 1974, 1985](#)) and
 156 later applications of it ([Lintunen & Vainio, 2004](#); [Laitinen et al., 2015](#); [L. Wang et al.,](#)
 157 [2011](#)), one implicit assumption is that electron motion in the IMF can be approximated
 158 by scatter-free propagation. This is a reasonable assumption if electrons do not inter-
 159 act strongly with IMF turbulence and if electron mean free paths are longer than 1 au.
 160 Furthermore, as shown in the simulations by [Moradi and Li \(2019\)](#), when the IMF tur-
 161 bulence is small, electron path length is close to the field line path length. Moreover, the
 162 simulations by [Moradi and Li \(2019\)](#) also showed that the electron path length has lit-
 163 tle dependence on electron energy.

164 The basic procedure of FVDA was explained in [Zhao et al. \(2019\)](#). Two slightly
 165 different approaches were introduced in [G. Li, Zhao, et al. \(2020\)](#); [G. Li et al. \(2021\)](#) in
 166 obtaining the release time T_r . Here we clarify these two approaches in more detail as it
 167 is crucial for our study. These two approaches, which we name as Approach I and Ap-
 168 proach II will yield similar T_r when electrons of different energies are released simulta-
 169 neously at the Sun. When the release is energy dependent, however, Approach II should
 170 be used to obtain the release times. Whether or not the release time is energy depen-
 171 dent in a particular event can be judged by examining if the path length L obtained from
 172 the FVDA method is physically meaningful or not (a path length shorter than 1 au would
 173 be a non-physical path length). Below we outline the general procedure of the FVDA
 174 with a focus on explaining the differences of the two approaches.

175 The steps of FVDA are the following: for each energy channel E_i , we identify from
 176 the electron time intensity profile a time $t_i(\eta)$ that corresponds to an intensity that is
 177 a fraction η of the peak intensity. For each η , we then apply the VDA to obtain a re-
 178 lease time $T_r(\eta)$ and a path length $L(\eta)$ which are now functions of η . Assuming elec-
 179 trons of different energies are released simultaneously at the Sun, one can now take $\eta \rightarrow$
 180 0 and obtain $T_r(\eta \rightarrow 0)$ and $L(\eta \rightarrow 0)$ which represent estimates of the release time
 181 and path length. Comparing to the VDA, the FVDA makes use of the entire rising phase
 182 of the electron time intensity profile and the procedure of taking $\eta \rightarrow 0$ provides a self-
 183 consistent check and uncertainty measure for the resulting T_r and L .

In obtaining the release time of electrons, two approaches can be used. In Approach I, we consider $T_r(\eta)$ as a function of η and take the limit of $\eta \rightarrow 0$ directly to obtain $T_r(\eta \rightarrow 0)$. In Approach II, one first obtains the onset time t_i (for electron in the i -th energy bin) from the time intensity profile by taking $\eta \rightarrow 0$ and then obtains the corresponding release times at the Sun. To implement this approach, we approximate the $t_i(\eta)$ as a polynomial in η ,

$$t_i(\eta) = a\eta^2 + b\eta + t_i^0 \quad (1)$$

where t_i^0 is the onset time of the i -th energy channel (corresponding to $\eta = 0$). Using multiple $(\eta, t(\eta))$ pairs, we can fit the parameters a, b , and t_i^0 . Once the onset time is obtained, one can compute the release time T_r of electrons at the Sun from

$$T_r(E_i) = t_i^0 - L/(\beta_i c) \quad (2)$$

184 where E_i is the energy of the i -th bin (using median value), $\beta_i c$ is the speed of electron
 185 in i -th bin and L is an assumed path length. Note that L can be taken as $L(\eta)$ from the
 186 fitting and with $\eta \rightarrow 0$, but does not need to be. In fact, as shown in (Zhao et al., 2019),
 187 $L(\eta \rightarrow 0)$ can be smaller than 1 au in many events. Such a non-physical value is a di-
 188 rect consequence of (incorrectly) assuming that electrons of different energies are released
 189 simultaneously at the Sun. Clearly when $L(\eta \rightarrow 0) < 1$ au, we should use Approach
 190 II and use a more physical value of L in equation (2). Approach II of the FVDA method
 191 allows one to infer an energy-dependent release and obtaining the corresponding energy-
 192 dependent release times of energetic electrons at the Sun. As pointed out in G. Li et al.
 193 (2021), this was not possible in the traditional VDA method since electrons of all ener-
 194 gies are assumed to be released at the Sun simultaneously in the VDA.

195 A reasonable value of L to be used in equation (2) is the nominal Parker path length,
 196 which depends on the solar wind speed. Note that footpoint random walk can lead to
 197 meandering field lines and affect the field line path length. However, the work by Moradi
 198 and Li (2019); Bian and Li (2022) suggested that in the case of solar wind, the path length
 199 of meandering field line do not differ much from the nominal Parker value. In this study,
 200 we consider three different values of L in equation (2) when using Approach II (see dis-
 201 cussion below).

202 Note that for the cases with simultaneous release (i.e. release is energy-independent),
 203 T_r from Approach I and Approach II should be close if the meandering field line does
 204 not deviate much from the Parker field. Among the 29 events we examine in this work,
 205 three events have energy-independent release times of in-situ electrons at the Sun. In these
 206 three events, as expected, the release times from Approach I are found to be close to those
 207 obtained from Approach II and both close to the Parker field path length. This agree-
 208 ment provides a self-consistent check for our analysis.

209 Figure 1 shows the results of FVDA for four events which occurred on 2005-05-16,
 210 2002-08-20, 2003-01-13, and 2004-10-04, respectively. Using Approach II, the deduced
 211 T_r of in-situ electrons at the Sun are shown as blue, orange, and green circles for three
 212 different choices of the path length. The blue circles are for a path length from using Ap-
 213 proach I of FVDA. If the calculated L is smaller than 1 au, we set it to 1 au. The or-
 214 ange circles assume a path length given by a nominal Parker spiral field using an aver-

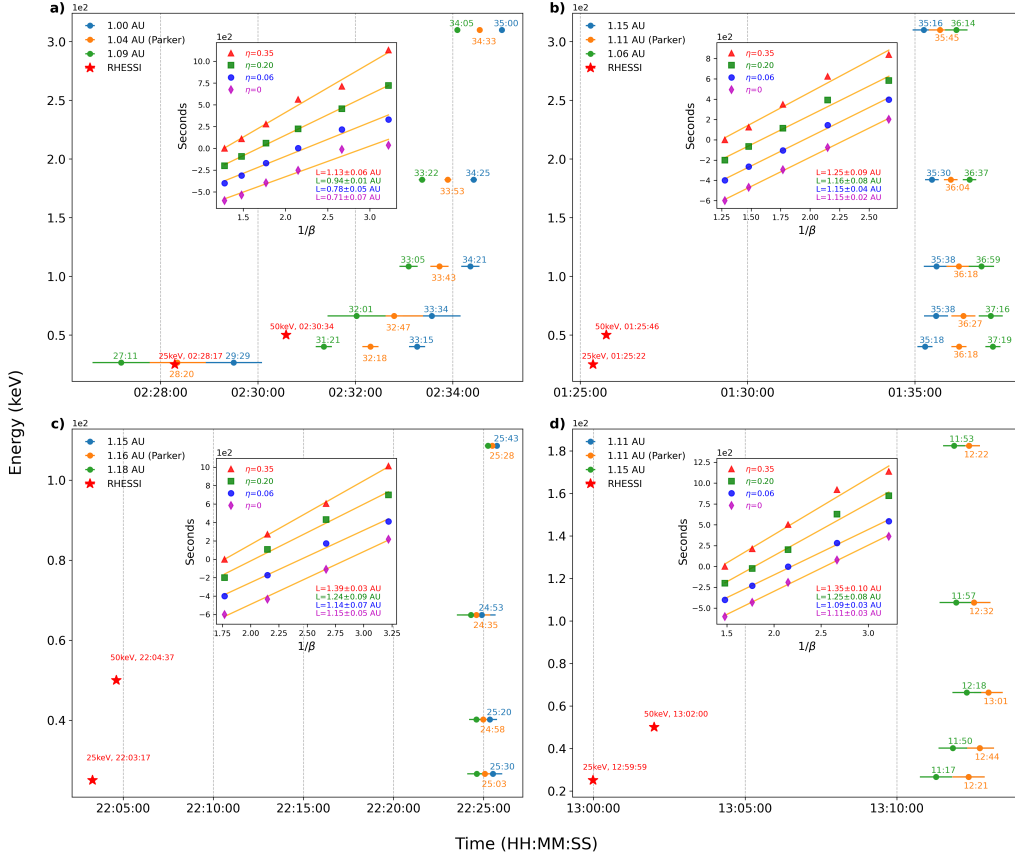


Figure 1. Electron release times as function of energy for four example events. In all panels, the Y-axis is electron energy, the X-axis is time. The green, orange and blue symbols correspond to three different path lengths used in equation (2) when using Approach II of FVDA. The red stars mark the start times of hard X-rays at the Sun. The insets in each panel show the FVDA plots for four different η s: 0.35, 0.20, 0.06, and 0 using Approach I of FVDA. See text for details.

215 age solar wind speed from a 12-hour window prior to the event. The green circles cor-
 216 respond to a complementary choice of path length to the blue and orange symbols. It
 217 is chosen such that it is longer (shorter) than the Parker path length if the blue sym-
 218 bol corresponds to a path length shorter (longer) than the Parker length; and the arith-
 219 metic average between the path lengths for the green and the blue symbols is the Parker
 220 path length. Hard X-ray start times at the Sun are marked by red stars. The inset in-
 221 side each panel are the FVDA analyses for $\eta = 0.35, 0.2, 0.06$ and 0 using Approach
 222 I. These are labeled as solid “triangle”, “square”, “circle”, and “diamond”, respectively.
 223 In panel a) of Figure 1, the release times of outward propagating electrons show a clear
 224 energy dependence, with electrons of higher energy released at a later time. This is con-
 225 sistent with the fact that the path length from Approach I is shorter than 1 au. For events
 226 in panels b), c), and d), the release times of outward electrons show little energy depen-
 227 dence. Indeed, using $L = L_{Parker}$ (corresponding to the orange symbols) T_r s for elec-
 228 trons of different energies are within one minute in all three events. Using the other two
 229 choices of the path length (green and blue symbols) still lead to an energy-independent
 230 release times. More over, the path lengths from Approach I in these three events are very
 231 close to the corresponding Parker field path lengths, indicating that the results from Ap-
 232 proach I and Approach II are similar. Note that in-situ electron data from the Wind/3DP

has a very refined time resolution of 12 s. In applying FVDA, we also apply the Savitzky-Golay filter with a window size of ~ 7 data points. For some events the data count for the 181 keV and 310 keV energy channels are low and a window size of ~ 11 second is used. Compared to the well-known boxcar averaging, the Savitzky-Golay filter estimates the sample value at the center of a window using a polynomial fitting (Savitzky & Golay, 1964; Baba et al., 2014). This helps to improve the signal-to-noise ratio of the data while preserving the position and width of the peaks, which is beneficial for our timing study. The Savitzky-Golay filter technique has been practiced in solar/heliospheric science before, see e.g., Williams and Pesnell (2011); Mitchell et al. (2020). Although the filter itself does not change the time resolution, it introduces a source of uncertainty in determining $t(\eta)$ and therefore the release time. We assume the uncertainty of $t(\eta)$ is 2.5 times the time resolution, which is 30 seconds in this work. Note that because the rising phase of the time intensity profile is very rapid, a change of $t(\eta)$ by 30 seconds often leads to a large change of η , suggesting that the uncertainty of $t(\eta)$ is likely smaller than 30 seconds.

In this work, to judge if the outward propagating electrons are released simultaneously at the Sun, we use a 1-minute threshold. If the release time difference between any two energy channels in a given event is shorter than 1 minute, then that event is classified as an energy-independent release event; otherwise it is classified as an energy-dependent release event. With this criterion, three events are found to be energy-independent release events. They are shown in Figure 1 (panels b to d). If we relax the threshold from 1 minute to 2 minutes, the number of energy-independent release events will increase to 5, which we will discuss in subsection 3.3. Note that the occurrence rate of energy-independent release is low, only $3/29 \sim 10\%$ if using a 1-minute threshold, and $5/29 \sim 17\%$ if using a 2-minute threshold. Therefore using the traditional VDA analysis in impulsive events would be inappropriate, and FVDA should be used.

3 Results and Discussion

As discussed in the last section, a total of 29 events were identified in our study. These events are listed in Table 1. Columns 1 and 2 are the event number and date of the events. Columns 3 to 6 contain the HXR onset/peak times observed by RHESSI at the 12–25 and 25–50 keV energy channels. Note that the HXR times are the observed time at 1 au and have not been corrected for the travel time. As in G. Li, Zhao, et al. (2020), we use the hard X-ray energy as a proxy for that of the parent electrons. The intensity profile of the HXR are the energy-integrated solar atmosphere response to the precipitating energetic electrons. To obtain the onset time of HXR, we first identify a background period (~ 5 to 10 minutes) before the event, then for each energy channel, the onset time of HXR is obtained as the time when the photon intensity is 3σ above the background. We use this time as the estimate for the release time of downward-propagating electrons. Column 7 contains times of type III radio bursts near the Sun. The times have been corrected for the travel time based on the location of the spacecraft, and they are to be compared with the release times of the in-situ electrons at the Sun. Columns 8–13 contain the release times of electrons for 6 energy channels from 26.6 to 310 keV at the Sun using Approach II and assuming a path length corresponding to the nominal Parker field, as shown in column 14. Columns 15 is the path length obtained from Approach I. Column 16 is the flare class of the event. Column 17 is the NOAA designated Active Region numbers of the flare events. This information is obtained from the HelioPhysics Event Knowledgebase (HEK) through SUNPY *hek* module https://docs.sunpy.org/en/stable/guide/acquiring_data/hek.html. If no data is available for a given event, this field is left blank.

Solar energetic electron events are often accompanied by type III radio bursts (L. Wang et al., 2012). Since the propagation of radio waves in the solar wind is not affected by the IMF, type III radio bursts can provide valuable information on electron release times.

285 However, a one-to-one association between type III radio bursts and in-situ electron events
 286 can be subject to large uncertainty due to the following. First, a single solar eruption
 287 may consist of multiple type III radio bursts, leading to ambiguity in the association be-
 288 tween type III radio bursts and in-situ electrons. Second, the generation of type III de-
 289 pends on many factors, and not all energetic electron beams may generate type-III ra-
 290 dio bursts (Cairns et al., 2018). In our work, of all 29 events, event 13 had no type III
 291 radio observation. This is possible if the electron streams did not excite radio waves (Cairns
 292 et al., 2018). For the rest 28 events, eleven events: 1, 2, 4, 7, 12, 16, 18, 21, 23, 24, and
 293 28 had only single type III radio bursts, so the identification of type III bursts in these
 294 events was unambiguous. The remaining 17 events have multiple type III radio bursts
 295 associated and we identify the type III burst as the one whose release time is closest to
 296 the release time of the lowest energy in-situ electrons. With this choice, from Table 1
 297 we can see that the release times of the outward-propagating electrons from our FVDA
 298 are consistent with the type III release times in 15 of 28 events. In these events, the time
 299 differences between the onset time of type III bursts and electron release time are within
 300 1 minute, suggesting that the type-III-radio-burst-generating electrons and the in-situ
 301 electrons are of the same population. These are events 2, 6, 10, 12, 15, 16, 17, 20, 21,
 302 22, 24, 26, 27, 28, and 29. Note that previous studies (Krucker et al., 1999; Haggerty &
 303 Roelof, 2002) have found that only a small percentage of the events they studied showed
 304 no delay between the inferred release times of the in-situ electrons and the type III ra-
 305 dio bursts. However, in these studies, the release times of in-situ electrons are obtained
 306 from the traditional VDA method, which, as pointed out by Zhao et al. (2019), is sub-
 307 ject to large uncertainties since the onset time of in-situ electrons can be hard to obtain.
 308 Here, using FVDA, we found that the type-III radio bursts (or one episode of multiple
 309 bursts) in more than half events coincide with the release of in-situ electrons. For the
 310 rest 13 events, except events 8 and 14, the release times of type III radio bursts are ear-
 311 lier than the release times of in-situ electrons. It is possible that in these events the type-
 312 III radio bursts are excited by other streams of energetic electrons. Incidentally, we note
 313 that in events 1, 3, 9, 18, 19, and 25, the onset times of type III radio bursts are within
 314 8-minute of the electron release time. An 8-minute window has been identified by L. Wang
 315 et al. (2006) who found the injection time of electrons at 13-300 keV was 7.6 ± 1.3 min-
 316 utes later than the type III radio bursts in impulsive electron events. In the rest 5 events
 317 (events 4, 5, 7, 11, and 23), the type III bursts precede the in-situ electrons by more than
 318 10 minutes.

319 It is interesting to note that for the 11 events where type III radio bursts precede
 320 the release of in-situ electrons, 7 events, events 4, 7, 9, 11, 18, 23, and 25, have the re-
 321 lease times of type-III radio bursts consistent (within 1 minute) with the release time
 322 of HXR. Without observations of in-situ electrons, this observation may suggest that
 323 the HXR-generating electrons and the type-III-radio-bursts-generating electrons are of
 324 the same population. However, note that type-III radio burst is only a proxy of low en-
 325 ergy (10-20 keV) electrons, and, as one can see from Table 1, the release of in-situ elec-
 326 trons in most events is energy dependent, so a more plausible scenario in these events
 327 could be the following: an interchange reconnection happens and leads to upward and
 328 downward propagating exhausts. Electrons with energy up to 10 to 20 keV are accel-
 329 erated near the initial X-point. Further acceleration at both reconnection exhausts leads
 330 to electrons of higher energy. For the exhausts propagating downward, the B field and
 331 associated turbulence are stronger, so the acceleration time is short leading to no clear
 332 energy dependence of HXR. For the exhausts propagating upward, however, the B field
 333 and associated turbulence are weaker, so the acceleration time is longer, leading to a clear
 334 energy-dependent release of in-situ electrons. In this scenario, the timing of type III ra-
 335 dio bursts can be the same as the hard X-ray if the initial X-point acceleration can ac-
 336 celerate electrons to 10 to 15 keV, the energy threshold for generating type III radio bursts.
 337 If the initial acceleration at the X-point is not powerful enough, then the type III bursts
 338 would be later than HXR. Nevertheless, because the upward propagating exhausts is
 339 associated with further acceleration, we can regard electrons that generate type III ra-

340 dio bursts and those that generate HXR as different populations. Indeed, an examina-
 341 tion of event 9 suggests that this may be the case. In event 9, there are three episodes
 342 of type III bursts. The middle episode has a release time of 03:10:53. In comparison, the
 343 release time of the 25 keV HXR is 03:09:57; the release time of 26.6 keV in-situ electrons
 344 is 03:12:25; and the release time of 40.2 keV in-situ electrons is 03:15:11. So the type III
 345 radio burst release time is ~ 1 minute later than the 25 keV HXR, and is ~ 1.5 min-
 346 utes earlier than the 25 keV in-situ electrons. Since type III radio bursts and 25 keV HXR
 347 are within 1 minute, one may regard them to be due to electrons of the same popula-
 348 tion. However, if the type III radio burst is generated by 15 – 20 keV electrons, then
 349 it is not clear why the type III burst trails the 25 keV HXR. On the other hand, the
 350 type III burst is only 1.5 minutes earlier than 26.6 keV in-situ electrons. Comparing to
 351 the fact that 26.6 keV in-situ electrons are 2.8 minutes earlier than the 40.2 keV in-situ
 352 electrons, it is more likely that the type-III generating electrons are of the same popu-
 353 lation as those in-situ electrons, and they lay behind the HXR-generating electrons. Event
 354 18 is similar to event 9. In event 25, the release of in-situ electrons also show clear en-
 355 ergy dependence, similar to event 9 and 18, but the 26.6 keV electrons are released \sim
 356 6 minutes than the type III radio bursts. These three events are further examined in sec-
 357 tion 3.2. For the other 4 events, events 4, 7, 11, and 23, type III bursts had no nearby
 358 in-situ electrons identified. This is possible if Earth is not magnetically connected to the
 359 flare source. Finally, we note that if the initial reconnection is via a closed-closed recon-
 360 nection and if it triggers an interchange reconnection, as discussed in [G. Li et al. \(2021\)](#)
 361 (see also later the Discussion section), then the type III radio bursts will also be trail-
 362 ing the HXR. In passing, multiple episodes of electron acceleration are likely a common
 363 feature of solar flares ([Sharma et al., 2020](#)). These authors also suggested that HXR and
 364 radio burst sources are likely from electrons in different magnetic loops.

365 Table 1 contains the main results of our work. In the following, we examine the time
 366 delays between the outward and the downward propagating electrons in subsection 3.1
 367 and discuss the energy dependence of the outward propagating electrons in subsection 3.2.
 368 Finally, in subsection 3.3, we examine one of the three simultaneous release events in de-
 369 tail.

370 3.1 Time delay between outward and downward propagating electrons

We examine the time delay Δt between the outward propagating electrons and the
 downward propagating electrons, which is defined as,

$$\Delta t = t_{o.e.} - t_{HXR} \quad (3)$$

371 where $t_{o.e.}$ is the release time of outward propagating electron from the FVDA (Approach
 372 II) and t_{HXR} is the release time of hard X-ray (as a proxy of release time of downward
 373 propagating electrons). Figures 2 and 3 show the time delay distribution for events in
 374 Table 1.

375 As an estimate of uncertainty, for the downward propagating electrons we use both
 376 the 12 – 25 keV and the 25 – 50 keV channel of HXR data and Figure 2 (Figure 3) is
 377 for the 12 - 25 keV (25 - 50 keV) HXR.

378 Consider first Figure 2. Different panels are for different electron energies. In each
 379 panel, the x-axis is the time delay Δt in seconds and the y-axis is the flare class. Dif-
 380 ferent events are marked by the green circles with the event number labelled next to it.
 381 Events 14 and 15 are marked by red circles since there is a lack of corresponding flare
 382 class information in these two events. In Figure 2, these two events are assigned a B2.0
 383 for clear presentation. Note that the number of events differ in these panels since not
 384 all events have in-situ electron observations from all six channels. The light blue histogram
 385 shown in the inset of each panel is the frequency distribution of the delay time.

Table 1. Event List

id	Date	HXR 12-25keV		HXR 25-50keV		Type III [†]	Tr of electrons (keV)						Path length		Class	AR	Note
		onset	peak	onset	peak		26.6	40.2	66.3	108.6	182.4	310	Parker	FVDA			
1	2002-05-06	23:42:58	23:56:56	23:55:31	23:56:56	23:43:33	23:51:06	23:52:46	23:53:56	23:53:03			1.17	0.99 ± 0.092	C6.4		
2	2002-07-18	23:12:17	23:15:12	23:13:05	23:15:12	23:54:30	23:54:32	23:55:01	23:55:37	23:56:26			1.17	1.02 ± 0.022	C8.2		
3	2002-08-20	01:33:42	01:40:20	01:34:06	01:40:16	01:30:39	01:36:19	01:36:27	01:36:19	01:36:04	01:35:45		1.11	1.15 ± 0.022	M5.0	10069	*a
4	2002-08-20	08:24:36	08:26:00	08:24:44	08:25:36	08:16:36	08:28:33	08:28:35	08:28:40	08:27:59	08:27:46		1.11	1.18 ± 0.033	M3.4	10069	
5	2003-01-13	22:11:37	22:15:40	22:12:56	22:15:44	22:13:50	22:25:04	22:24:58	22:24:35	22:25:29			1.16	1.15 ± 0.048	C2.1		*a
6	2003-07-08	02:17:16	02:17:48			02:17:39	02:16:21	02:17:45	02:18:27	02:20:47			1.10	0.76 ± 0.072	C2.3	10397	
7	2003-07-09	16:26:44	16:31:48			16:17:55	16:46:41	16:52:04	16:55:35	17:00:03			1.14	0.07 ± 0.070	C5.8	10397	
8	2003-10-04	13:08:18	13:14:40	13:10:19	13:16:40	13:14:45	13:12:22	13:12:44	13:13:01	13:12:33	13:12:23		1.11	1.11 ± 0.027	C2.5		*a
9	2004-02-28	03:18:16	03:19:08	03:18:05	03:18:24	03:10:53	03:12:25	03:15:11	03:17:20	03:18:31	03:18:44		1.18	0.73 ± 0.048	B6.6	10564	
10	2004-07-24	18:22:52	18:26:44			18:36:31	18:36:51	18:38:13	18:38:04	18:39:19			1.08	0.90 ± 0.054	C1.1	10652	
11	2004-11-01	03:17:36	03:20:08	03:17:45	03:19:00	03:09:53	03:19:20	03:21:13	03:21:15	03:20:17	03:21:37		1.13	1.03 ± 0.070	M1.1	10691	
12	2005-05-16	02:36:36	02:41:28	02:38:53	02:40:16	02:31:41	02:28:21	02:32:19	02:32:48	02:33:44	02:33:54	02:34:33	1.04	0.71 ± 0.067	M1.4	10763	
13	2005-09-04	15:10:25	15:11:52	15:10:23	15:13:44		15:00:09	15:02:09	15:02:16	15:02:10			1.06	0.85 ± 0.090	C2.0	10803	*b
14	2006-11-19	22:54:23	23:02:40	22:52:13	23:03:48	22:51:46	22:48:26	22:50:14	22:49:09	22:50:30	22:52:44		1.16	0.93 ± 0.096			
15	2006-11-20	03:34:10	03:35:36			03:26:49	03:24:44	03:27:05	03:28:05	03:29:07			1.17	0.73 ± 0.034			
16	2006-11-21	08:28:52	08:29:16			08:20:53	08:19:49	08:20:27	08:21:08	08:22:33			1.21	0.95 ± 0.062	B2.3		
17	2006-11-21	16:17:14	16:20:12			16:41:44	16:40:26	16:41:55	16:42:36	16:44:43			1.20	0.87 ± 0.061	B3.3		
18	2011-05-15	23:28:23	23:31:02	23:29:24	23:31:02	23:20:39	23:22:14	23:25:55	23:28:19	23:29:12	23:29:03		1.10	0.61 ± 0.087	C4.8	11208	
19	2011-07-31	19:03:58	19:06:28	19:04:42	19:04:44	18:57:04	18:59:44	19:00:44	19:02:46	19:03:26			1.07	0.74 ± 0.037	C1.7	11265	
20	2011-08-08	15:31:55	15:35:09	15:34:02	15:35:05	15:51:00	15:52:30	15:55:21	15:55:50	15:57:49			1.09	0.69 ± 0.075	B8.1	11263	
21	2011-08-09	08:00:23	08:04:04	08:00:34	08:03:44	07:54:39	07:54:23	07:56:56	07:59:11	07:59:52	08:00:13	08:00:13	1.07	0.71 ± 0.051	X6.9	11263	
22	2012-09-27	23:47:14	23:48:06	23:47:26	23:48:06	00:06:46	00:09:35	00:09:35	00:06:41	00:07:37	00:05:18	00:05:16	1.15	1.51 ± 0.097	C3.7	11577	
23	2013-11-13	10:30:26	10:31:52	10:30:46	10:31:48	10:22:52	10:36:35	10:37:31	10:38:46	10:40:26			1.16	0.85 ± 0.046	C3.5	11890	
24	2014-02-20	07:40:00	07:49:08	07:40:53	07:45:20	07:40:03	07:39:49	07:43:40	07:45:49	07:46:50	07:47:10		1.10	0.59 ± 0.075	M3.0	11976	
25	2014-03-28	23:45:13	23:49:35	23:48:15	23:49:07	23:39:34	23:46:00	23:47:53	23:49:25	23:50:07	23:50:06		1.14	0.85 ± 0.041	M2.6	12017	
26	2014-06-12	10:48:42	10:49:13	10:48:46	10:49:13	10:48:44	10:49:15	10:49:54	10:50:44	10:50:04			1.10	1.02 ± 0.054	M2.7	12085	
27	2014-06-12	13:10:49	13:14:32			13:13:40	13:13:40	13:15:30	13:16:10	13:17:02	13:17:32	13:17:46	1.11	0.86 ± 0.020	C3.8	12080	
28	2016-07-20	22:03:32	22:11:52	22:05:01	22:06:52	21:56:27	21:54:37	21:57:17	21:58:35	21:58:55	21:59:30	21:59:57	1.10	0.79 ± 0.040	C4.6	12567	
29	2016-07-23	05:06:32	05:15:00	05:09:07	05:10:40	05:02:04	05:02:15	05:05:03	05:06:58	05:07:44	05:08:42	05:09:13	1.14	0.74 ± 0.030	M7.6	12567	

a: energy-independent release of in-situ electrons.

b: the HXR onset times can be delayed from the real values due to data gap.

†: the propagation time has been subtracted from the time of type III radio bursts.

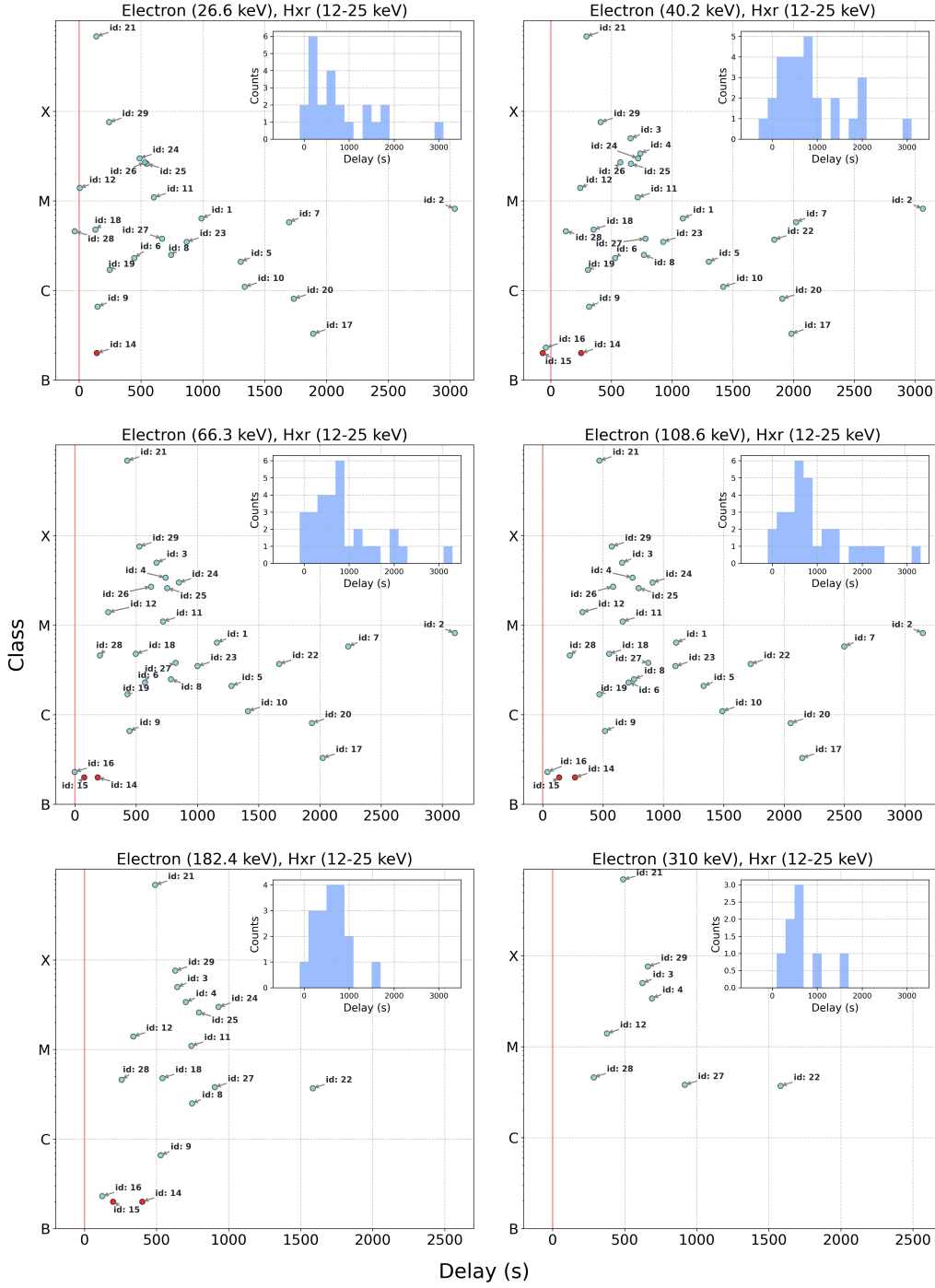


Figure 2. Time delay of the release time of in-situ electrons from the release time of the 12 – 25 keV channel of HXR. Note that both are release times at the Sun. X-axis is the delay time in seconds; and the Y-axis is the flare class. Events number are shown next to the data point. For events 14 and 15, no flare class information were available and an arbitrary B2.0 was assigned. They were labelled by filled red circles.

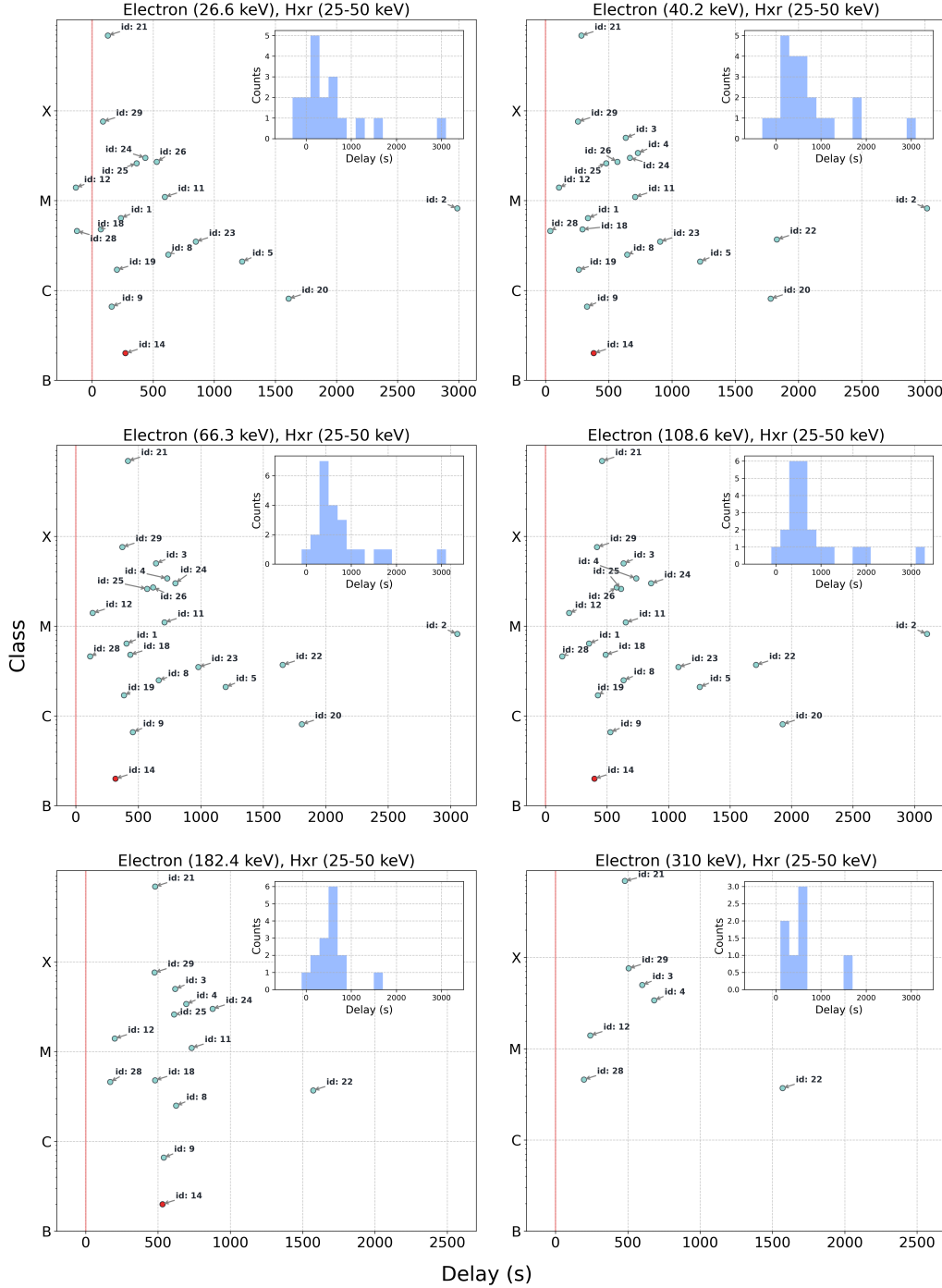


Figure 3. Same for Figure 2, but using the 25 – 50 keV channel instead of the 12 – 25 keV channel of HXR to compute the release time delay.

386 From Figure 2 we see that the release time of outward propagating electrons in all
 387 events and all energy channels lag behind the 12 - 25 keV HXR release time except events
 388 15, 16 and 28 (see below). The delay is mostly distributed within 1000 seconds, with a
 389 few events having a delay beyond 2000 seconds and one event (event 2) having a delay
 390 of ~ 3100 seconds.

391 For event 15, in-situ electron data exist only for four energy channels. Of these, only
 392 the 40.2 keV electrons are found to be released earlier than the 12-25 keV HXR. The re-
 393 lease time of the 40.2 keV electrons is 03:24:44, with a $\sim 30 + 42$ s uncertainty, where
 394 30 is the intrinsic uncertainty from using the the Savitzky-Golay filter and 42 is the un-
 395 certainty from the fitting. The release time of 12-25 keV HXR is 03:25:50, with a ~ 12 s
 396 (a smoothing window size of 3 times the time resolution of 4 seconds) uncertainty. There-
 397 fore, the release time delay between the 40.2 keV electrons and the 12-25 keV HXR is
 398 consistent with 0. As energy increases, the release times of outward propagating elec-
 399 trons become clearly delayed from that of the HXR. For event 16, in-situ electron data
 400 is also only available for 4 energy channels. The deduced release time of 12 - 25 keV HXR
 401 is 08:20:33, and the earliest T_r of outward electrons is from the 40 keV channel, which
 402 is 08:19:48. This yields a delay time of ~ -45 s. Considering that the uncertainty of in-
 403 situ electrons of 40 keV is $\sim 30 + 18$ s, and the uncertainty for HXR observation is 12
 404 seconds, this time delay is also consistent with 0. Furthermore, as energy increases, the
 405 release times of outward propagating electrons become clearly delayed from that of the
 406 HXR, as in event 15. For event 28, in-situ electron data is available for 6 energy chan-
 407 nels. All in-situ electrons except the 26.6 keV channel are released later than the 12-
 408 25 keV HXR. The release time for the 26.6 keV outward electron is 21:54:37 with un-
 409 certainty $\sim 30 + 13$ s, and that of the 12-25 keV HXR is 21:55:13 with uncertainty 12
 410 s. Again, taking into account of uncertainty, the time delay is also consistent with 0. For
 411 the other 5 energy channels, the release time of the outward electrons are again signif-
 412 icantly later than that of the HXR, similar to event 15 and 16. Therefore, we can con-
 413 clude that, in these three events, the outward propagating electrons of lower energy (40
 414 keV in event 15 and 16, 26.6 keV in event 28) are released close in time with the 12-25
 415 keV HXR, and electrons of higher energies (> 40 keV) show clear delays from the HXR.

416 Figure 3 is similar to Figure 2 but using 25 – 50 keV HXR when calculating the
 417 time delay. In only two events we find that the outward propagating electrons in the en-
 418 ergy channel of 26.6 keV are released earlier (~ 2 minutes in both events) than the 25-
 419 50 keV HXR. These are event 12 and 28. However, for > 50 keV outward propagating
 420 electrons, they are all delayed from the 25-50 keV HXR. The delays are again mostly
 421 within 1000 seconds. From Figure 2 and Figure 3, we can conclude that in nearly all events
 422 we examine, the outward propagating electrons are delayed from the downward prop-
 423 agating electrons of the same energy, and the delay is largely within 1000 seconds.

424 Comparing Figure 2 with Figure 3, we also see that the downward-propagating elec-
 425 trons themselves may be released in an energy-dependent manner. In fact, from Table 1,
 426 the downward-propagating electrons of 25 – 50 keV in event id = 5, 8, 18, 20, 25, 28,
 427 and 29 show a clear delayed release relative to those of 12–25 keV, indicating that the
 428 acceleration process of the downward electrons may be also time dependent. This is pos-
 429 sible, e.g., if the downward propagating electrons are accelerated at a flare termination
 430 shock (G. Li et al., 2013; Guo et al., 2017).

431 To summarize, except for event 13 where an accurate HXR release time can not
 432 be obtained due to a data gap, the outward-propagating electrons of all energy channels
 433 in the rest of the 28 events are released consistently later than the downward-propagating
 434 HXR-generating electrons. The delay between the outward propagating electrons and
 435 the downward propagating electrons is largely within 1000 seconds. This statistical re-
 436 sult can be naturally explained if the acceleration sites of outward- and downward-propagating
 437 electrons are different. Different acceleration sites could be the two oppositely propagat-
 438 ing reconnection exhausts as proposed in Liu et al. (2013), or for the outward propagat-
 439 ing electrons, a shock wave driven by the jet can be an additional acceleration site be-
 440 sides the reconnection exhaust (G. Li, Zhao, et al., 2020). Note that the fact that the de-
 441 lays are largely within 1000 seconds suggests that the acceleration time scale of the out-
 442 ward propagating electrons is < 1000 seconds. If a CME-driven shock is involved, as-
 443 suming a shock speed of $\sim 700 - 1400$ km/s, the shock moves a distance of $1 - 2R_s$ in

1000 seconds. So the acceleration of outward propagating electrons occurs within a few solar radii.

3.2 Energy-dependent release of outward propagating electrons

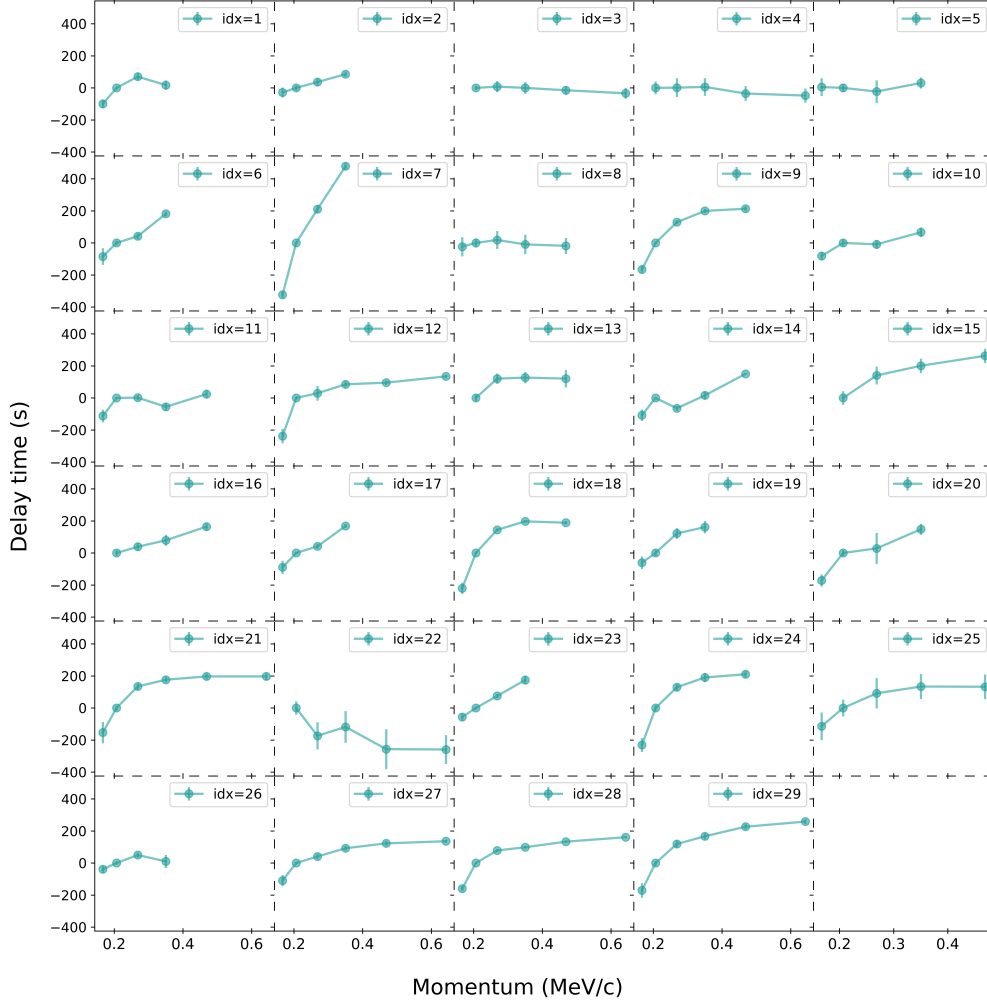


Figure 4. The momentum-dependent time delay $\Delta t(p, p_0)$ of outward propagating electrons with respect to p_0 . To unify the reference point for all events, p_0 is chosen to be 0.207 MeV/c (i.e., $E_0 = 40.2$ keV). Data points are marked as cyan circles. The x-axis is electron momentum in unit of MeV/c and the y-axis is the time delay in seconds. The uncertainty of the $\Delta t(p, p_0)$ is the sum of the uncertainty in the release time of the electron with momentum p and the electron with momentum p_0 .

In this subsection, we examine the energy dependence of the release time of outward propagating electrons. As explained in the previous subsection, if the electron release times of any two different energies are within one minute, the event is classified as an energy-independent release event (which we discuss in the next subsection), otherwise it is classified as an energy-dependent release event. With this criterion, events 3, 5, and 8 are the only three energy-independent events. The release times for in-situ elec-

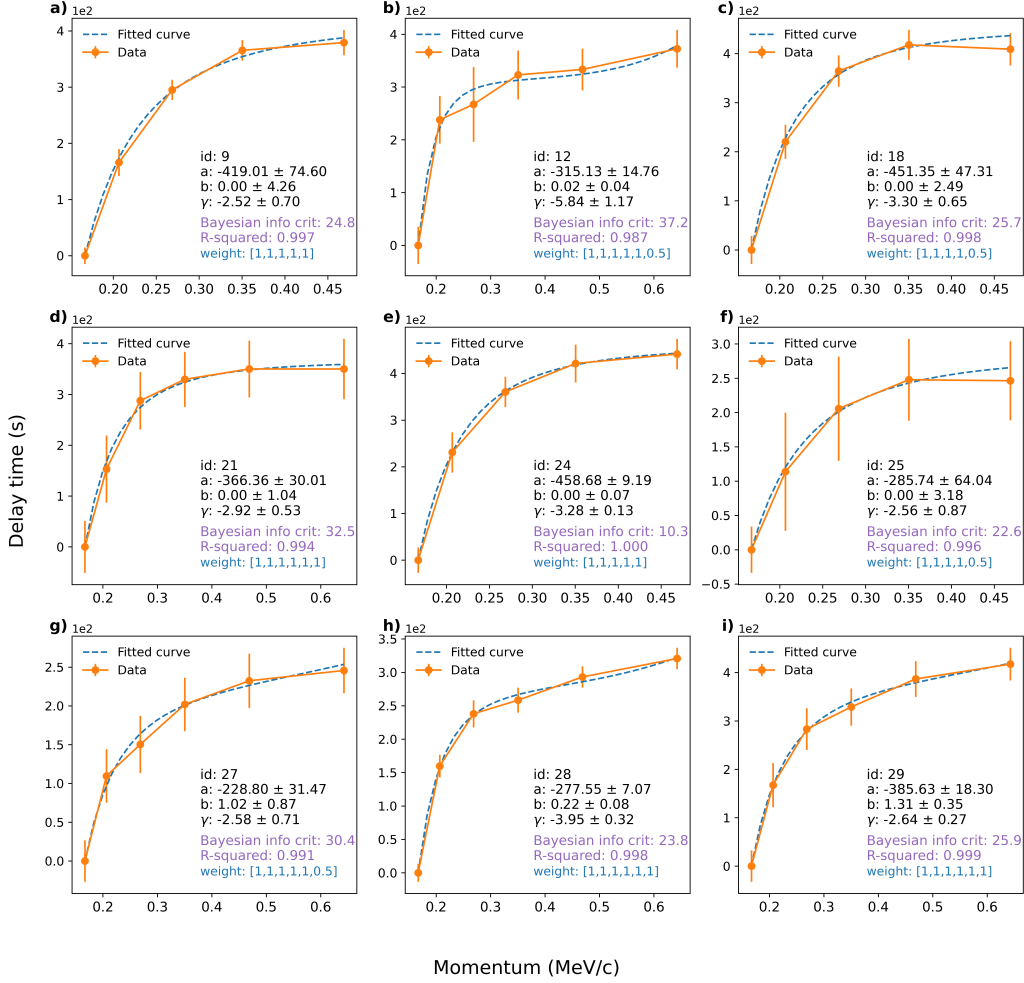


Figure 5. The momentum dependence of the release time difference $\Delta t(p, p_0)$ with $p_0 = 0.167$ MeV/c. Only events with 5 or more data points are fitted. The orange filled circle are the data and the blue dashed line is the fitting. The x-axis is electron momentum in unit of MeV/c and the y-axis is the time difference in seconds (note that the y-axis values are to be multiplied by a factor of 100, as indicated in the upper left corner of the panels). The uncertainty of the $\Delta t(p, p_0)$ is the sum of the uncertainty in the release time of the electron with momentum p and the electron with momentum p_0 .

trons using the FVDA methods for these three events were included in section 2. Note that relaxing this threshold from 1 minute to 2 minutes will increase the number of energy-independent release events to 5. Besides events 3, 5, and 8, events 4 and 26 also become energy-independent release events. More discussions on these events will be given in the next subsection.

In the work of [G. Li et al. \(2021\)](#), the release times of electrons at different energies (thus different momenta) are compared with that at a reference momentum p_0 to yield the release time difference $\Delta t(p, p_0) = t_{rel}(p) - t_{rel}(p_0)$. We follow [G. Li et al. \(2021\)](#) in obtaining the release time difference $\Delta t(p, p_0)$. Figure 4 shows the momentum dependence of the time difference $\Delta t(p, p_0)$ for all 29 events. The reference momentum p_0 is 0.207 MeV/c for all events. In Figure 4, the error bar of each point represents the

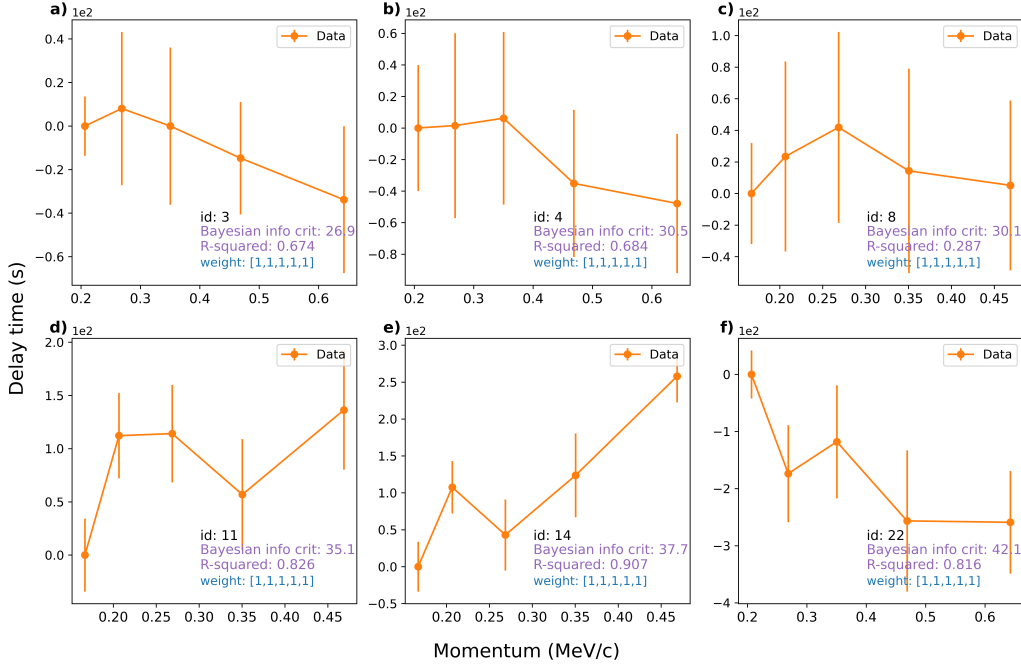


Figure 6. Similar to Figure 5, but for events that can not be fitted by equation (4).

464 uncertainty derived from electron release times. Assuming the release time of electrons
 465 is $t_r(p) = t(p) \pm u(p)$, the time difference can be expressed as $\Delta t(p, p_0) = (t(p) - t(p_0)) \pm$
 466 $(u(p) + u(p_0))$, where p_0 corresponds to the reference momentum and $(u(p) + u(p_0))$
 467 represents the deduced uncertainty of $\Delta t(p, p_0)$. We can see that the uncertainty of the
 468 time delay for most points is smaller than the data symbol. For the majority of these
 469 points, the uncertainty is smaller than 60 seconds.

As can be seen from Figure 4, $\Delta t(p, p_0)$ for many events show similar momentum
 dependence. Assuming this time difference is caused by acceleration and trapping, G. Li
 et al. (2021) has proposed to fit the release time difference as a function of electron mo-
 mentum by,

$$\Delta t(p, p_0) = \text{sign}(\gamma) a \left[\left(\frac{p}{p_0} \right)^\gamma - 1 \right] + b \left[\left(\frac{p}{p_0} \right)^{-\gamma} - 1 \right]. \quad (4)$$

470 Here p is the momentum of electrons, p_0 is the reference momentum and is chosen to be
 471 the lowest energy channel for a given event. According to our event list, the lowest en-
 472 ergy of electrons for an event is either 26.6 keV (corresponding to $p_0 = 0.167$ MeV/c)
 473 or 40.2 keV (corresponding to $p_0 = 0.207$ MeV/c). In the right side of equation (4), the
 474 1-st term is due to acceleration, and the 2nd term is due to escape/trapping, both of which
 475 are functions of the spatial diffusion coefficient $\kappa(p)$, which we assume to have momen-
 476 tum dependence as $\sim p^\gamma$ (G. Li et al., 2021). If we further assume the spectrum of the
 477 broad-band turbulence can be approximated as $\kappa^{-\epsilon}$, then under the framework of quasi-
 478 linear theory (Jokipii, 1966), the spectral index ϵ satisfies $\gamma = 3 - \epsilon$. Hence, we can
 479 probe the nature of the turbulence at the flare site using the fitting parameter γ .

480 Equation (4) contains four parameters: p_0 , a , b and γ , therefore to have a mean-
 481 ingful fitting, we only consider events with five or more data points, leading to a total
 482 of 15 events (see Figure 4). Of these, 9 events can be fit reasonably well by equation (4)
 483 and these are shown in Figure 5. The remaining 6 events do not yield reasonable fitting
 484 and are shown in Figure 6.

Table 2. The fitted γ value as in equation (5).

id	Date	γ^*	Class	R^2	Bic
9	2004-02-28	-2.52 ± 0.70	B6.6	0.997	24.8
12 [†]	2005-05-16	-5.84 ± 1.17	M1.4	0.987	37.2
18	2011-05-15	-3.30 ± 0.65	C4.8	0.998	25.7
21 [†]	2011-08-09	-2.92 ± 0.53	X6.9	0.994	32.5
24	2014-02-20	-3.28 ± 0.13	M3.0	1.000	10.3
25	2014-03-28	-2.56 ± 0.87	M2.6	0.996	22.6
27 [†]	2014-06-12	-2.58 ± 0.71	C3.8	0.991	30.4
28 [†]	2016-07-20	-3.95 ± 0.32	C4.6	0.998	23.8
29 [†]	2016-07-23	-2.64 ± 0.27	M7.6	0.999	25.9

* $P_0 = 0.167 \text{ MeV}/c, \eta = 0$.

† Events with six data points.

485 In Figure 5, the data is shown as the orange dot and the fitted curve is shown as
486 the blue dashed line. The coefficient of determination (R^2) and the Bayesian informa-
487 tion criterion (BIC) are also obtained. Both R^2 and BIC are indicators of the goodness
488 of the fitting. The range of R^2 is from 0 to 1 and $R^2 = 1$ represents a perfect fitting.
489 We require R^2 to be larger than 0.98 to consider it an acceptable fitting. The BIC is a
490 useful statistical measure for model selection, taking overfitting into account. When mul-
491 tiple models (often of similar kind but with different parameters) are adopted for a fit-
492 ting, the one with lower BIC is generally preferred. In our fitting we examine how the
493 BIC varies by allowing the data points for different energy bins to have different weights.
494 This is to capture the fact that the quality of electron profiles for different energy bins
495 is different. Generally, the electron time intensity profiles of higher energy, e.g., 182.4
496 keV or 310 keV, have larger fluctuations than those at lower energies so that they may
497 correspond to a lower weight. For simplicity, the weight of each data point is set to be
498 either 1 or 0.5. If one tenth of the peak flux (corresponding to $\eta = 0.1$) is lower than
499 the average pre-event background $+3\sigma$, a weight of 0.5 will be assigned to that energy
500 channel. Otherwise, the weight is set to be 1. Whether or not the weight of a specific
501 delay time is set to 0.5, it has little impact on the value of γ . Taking panel g) as an ex-
502 ample, if we do not decrease the weight of the last data point, the value of γ becomes
503 -2.5 ± 0.68 from -2.58 ± 0.71 , the R^2 remains 0.991, and BIC changes to 30.6 from
504 30.4. This shows that the choice of a non-uniform weight does not affect our fitting re-
505 sult, indicating the robustness of the fitting results.

In all panels of Figure 5, the parameter b is consistent with 0, i.e., the delay due to trapping is negligible. This means that equation (4) can be simplified to be,

$$\Delta t(p, p_0) = \text{sign}(\gamma) a \left[\left(\frac{p}{p_0} \right)^\gamma - 1 \right]. \quad (5)$$

506 Clearly parameter a is an overall amplitude, and the shape of the curve is completed de-
507 cided by the parameter γ . The fitting result of γ for these 9 events are summarized in
508 Table 2. Events with six data points are marked by the “†” symbol.

509 Figure 6 is similar to Figure 5, but for events that can not be fitted by equation (4).
510 For these events, we find that although the uncertainty of the time delay $\Delta t(p, p_0)$ is smaller
511 than 60s, it is still relatively large compared to the value of $\Delta t(p, p_0)$. In events 3, 4, and
512 8, the uncertainty of the $\Delta t(p, p_0)$ exceed the value of $\Delta t(p, p_0)$, which implies that a clear
513 energy dependence of the release time for these events can not be obtained. Taking event
514 8 (corresponding to panel c) in Figure 6 as an example, electrons of 0.167 MeV/c (i.e.,

515 $E_0 = 26.6$ keV) are released at $13:12:22 \pm 32.0$ s, and electrons of 0.269 MeV/c (i.e.,
 516 $E_0 = 66.3$ keV) are released at $13:13:01 \pm 28.4$ s. The deduced time delay $\Delta t(0.269 \text{ MeV/c}, p_0)$
 517 with respect to $p_0 = 0.167$ MeV/c is therefore 39 ± 60.4 s. This means that within the
 518 uncertainty, electrons of these two energies are released simultaneously. In panel c) of
 519 Figure 6, all the data points have $\Delta t(p, p_0)$'s uncertainty greater than its value, there-
 520 fore the electrons of different energies can be regarded as released at the same time. This
 521 explains why the release times cannot be well-fitted by equations (4) or (5) for this event. In
 522 panel a) & b) have the same pattern with event 8 in panel c). In panel d) & e) of Figure 6,
 523 $\Delta t(p, p_0)$'s uncertainty becomes smaller than its value. Although elec-
 524 trons of higher energies are generally released later, the time delay is not a convex func-
 525 tion, but bends at a certain momentum above p_0 . This is possible if the diffusion coef-
 526 ficient does not have a momentum dependence given by p^γ or if the acceleration process
 527 is not governed by a diffusion process (e.g. it may be governed by a DC electric field ac-
 528 celeration).

529 Panel (f) of Figure 6 is event 22. Of all 29 events, event 22 is the only event in which
 530 high energy electrons are released earlier than low energy electrons when a nominal Parker
 531 field length is used. If one assumes, as in other events, that high energy electrons are re-
 532 leased at the same time or later than low energy electrons, then a path length longer than
 533 the nominal Parker field path length has to be assumed. In fact, the path length from
 534 Approach I for this event is 1.51 au. Using this path length, the release times between
 535 different energy channels are within 123 seconds. We note that the rising phases of elec-
 536 tron time intensity profiles in this event are much gradual than other events. This can
 537 be caused by distorted IMF due to a large scale structures in the solar wind, e.g. a pre-
 538 ceding CME, which can lead to a longer path length. Therefore it is possible that in this
 539 event, electrons are released similar in time and they propagate along a magnetic field
 540 that is non-Parker and having a path length ~ 1.5 au. Such a scenario is not unheard
 541 of, and has been discussed in [G. Li, Wu, et al. \(2020\)](#).

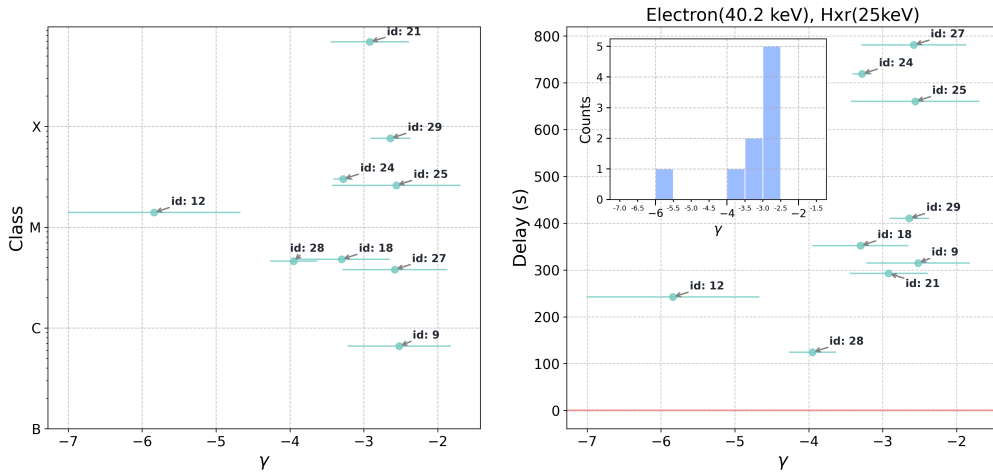


Figure 7. The distribution of the γ value for the 9 events shown in Table 2. The y-axis in the left panel is the flare class and the y-axis in the right panel is the relative release time delay $\Delta t(p, p_0)$.

542 The distribution of γ and its dependence on the solar flare class and the relative
 543 release time delay is shown in Figure 7. The light blue histogram in the right panel is
 544 the distribution of γ . The γ is mainly distributed between -3.5 and -2.5 , and shows no
 545 clear correlation with the flare class and the delay time. Event 12 has a $\gamma = -5.84$ which
 546 is significantly smaller than the gamma value of other 8 events. From Figure 5 we see

that event 12 has a $R^2 = 0.987$, the smallest of all 9 events in Figure 5. Since $\epsilon = 3 - \gamma$, we can infer that ϵ is mainly distributed between 5.5 and 6.5. As pointed out in G. Li et al. (2021), an ϵ steeper than 3 (corresponding to the nominal value for the dissipation range turbulence), is consistent with a scenario of magnetic reconnection in the reconnection exhaust. In the work of Vech et al. (2018), the authors found that the turbulence spectrum can be significantly steepened from 3 at the beginning of the dissipation range due to the generation of vortex-like structures, which are triggered by magnetic reconnection. This phenomenon of structure disruption significantly accelerates the turbulence cascading process, and to maintain a constant energy cascading rate a steeper spectrum must develop. These vortex-like structures can lead to large non-thermal velocity at the reconnection site. Using the Fe XXIV 192.03 Å line broadening, Y. Li et al. (2018) inferred a large nonthermal velocity in the SOL2017-09-10T16:06 flare, consistent with (Vech et al., 2018). Our result of a ϵ ranging between 5.5 to 6.5 also supports Vech et al. (2018). Note that event 29 was the event examined by G. Li et al. (2021). In G. Li et al. (2021), a $\gamma = 5.1$ was obtained. This is to be compared with this work where we find $\gamma = 5.64 \pm 0.27$. The difference is mainly due to the selection of the background. In G. Li et al. (2021) the background period was chosen to be the same for different energy channels for a fixed 10 minutes which was 05:18 ~ 05:28(HH:MM). This period however, overlaps with the rising phases for the 182 and 310 keV electrons. Consequently this leads to a smaller γ in (G. Li et al., 2021). In the current work, we use different background periods for different energy channels.

3.3 Energy-independent release of outward propagating electrons

If the electron release times of different energies in one event are within one minute, the event is classified as an energy-independent release event. Three events out of 29 events are energy-independent release events. These are event 3, 5, and 8 in Table 1. The release times of HXRs and in-situ electrons for these three events are shown in Figure 1. Because these events differ from the rest of the events, in the following, we take a closer look of both the remote sensing and in-situ observations of event 3 as an example.

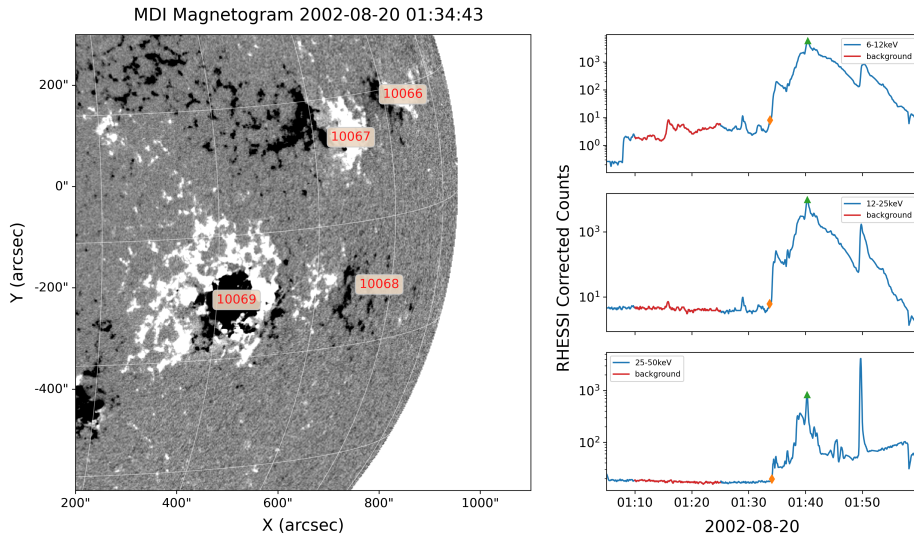


Figure 8. Left: Magnetogram of the 2002-08-20 event. The source region of the flare is AR10069. Right: the RHESSI HXR time profile. The background period is shown by the red segment.

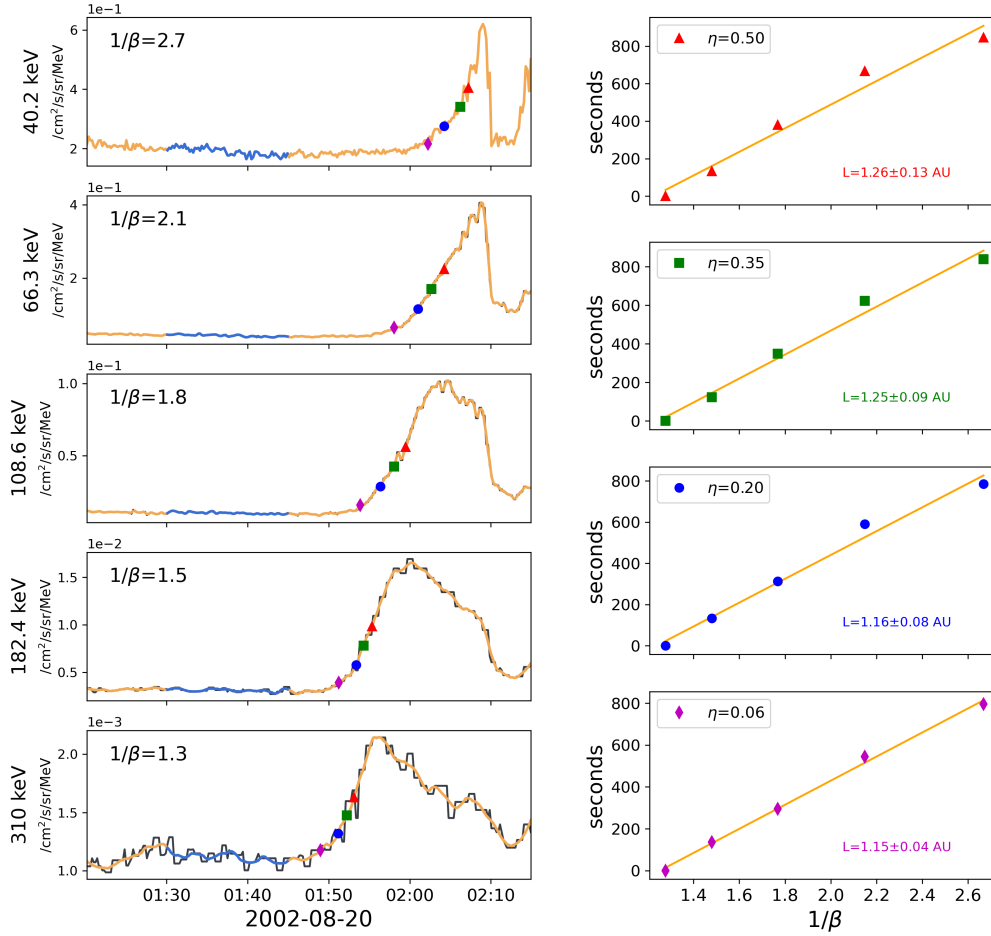


Figure 9. Left: in-situ electron time intensity of the 2002-08-20 event. Data for 5 energy channels are available for this event. Data from Wind/3DP is shown as the black curve and the yellow curve is after applying the Savitzky-Golay filter. For the two lowest energy channel, the black curve is overlapped by the yellow curve. Right: the FVDA results for four different η . As η decreases, the path length also decreases and approaches the nominal Parker field path length.

Figure 8 shows the magnetogram of the active region (AR) 10069 in the left panel, and the HXR intensity from 01:05 to 02:00 UT for three energy channels in the right panel. The active region is located at a longitude of western 40° , therefore is magnetically well connected to the Earth along the nominal Parker field (see below). In the right panel, the segments in red indicate the backgrounds from 01:10:00 to 01:25:00 UT. The onset and peak times of the HXR are labeled as the orange “diamond” and green “triangle”, respectively. The onset times for HXR-generating electrons of 12–25 and 25–50 keV are determined to be 01:33:42 and 01:34:06 UT.

In Figure 9, the left panel shows the electron time intensity profile for 5 energies. The reference points marked as “triangle”, “square”, “circle”, and “diamond” correspond to $\eta = 0.5, 0.35, 0.2, 0.06$, respectively. The right panel shows the FVDA analysis for the four η s. The nominal Parker field length of this event is 1.11 au with a solar wind speed $V_{sw} = 508.4$ km/s, the average of an 8-hour period that is two hours prior to the arrival of the in-situ electrons. Using equation 1, the onset times $t_0(\eta = 0)$ are 02 : 00 :

589 51 ± 13 s, $01 : 56 : 13 \pm 21$ s, $01 : 52 : 35 \pm 22$ s, $01 : 49 : 41 \pm 12$ s, and $01 : 47 : 30 \pm 20$ s for
 590 electron energies of 40, 66, 109, 182, and 310 keV, respectively. Therefore, the path length
 591 L calculated from $t_0(\eta = 0)$ is 1.15 ± 0.02 au, which is very close to the Parker value,
 592 suggesting that the field line in this event does not deviate much from the nominal Parker
 593 field. As shown in Figure 1, choosing a path length of 1.15 au and 1.06 au and using Equa-
 594 tion (2), we still find that the T_r for electrons of different energies are consistent with
 595 a simultaneous release.

596 An energy-independent release of outward propagating electrons could be due to
 597 a very fast electron acceleration directly at the magnetic reconnection site (see e.g. PIC
 598 simulations by X. Li et al. (2017)). It is tempting to invoke the interchange recon-
 599 nection scenario as proposed in Heyvaerts et al. (1977); Krucker et al. (2007) for this event.
 600 However, as shown in Figure 2 and Figure 3, there is a time delay (> 500 seconds) be-
 601 tween the outward and the downward propagating near-relativistic electrons, which is
 602 hard to explain if the interchange reconnection is responsible for both the downward and
 603 outward propagating electrons. One possible explanation of the delay is that a solar flare
 604 is intermittent and can have multiple episodes of magnetic reconnection and which can
 605 occur at different locations. The outward propagating electrons may correspond to one
 606 of many episodes but not the very first episode of the magnetic reconnection process. If
 607 the very first episode of the magnetic reconnection is of closed-closed reconnection in-
 608 stead of interchange reconnection, then there will be only HXRs associated with the first
 609 episode of the reconnection but not in-situ electrons. If a subsequent interchange recon-
 610 nection occurs and the open field line is magnetically connected to the earth, then elec-
 611 trons accelerated at the earlier closed-closed reconnection site can access these open field
 612 lines and be observed in-situ at 1 au. Indeed, recent observations of HXR and microwave
 613 suggested that multiple episodes in a solar flare are not uncommon (Battaglia et al., 2021;
 614 Sharma et al., 2020).

615 Event 3 has been examined previously by Krucker et al. (2007). In that study, the
 616 authors used the traditional VDA to obtain estimates of the release time of in-situ elec-
 617 trons at the Sun and an event is defined to be a prompt event if this release time coin-
 618 cides with the HXR burst time. Krucker et al. (2007) classified this event as a prompt
 619 event. However, the VDA method contains large uncertainty in obtaining the release time
 620 of in-situ near-relativistic electrons at the Sun. In this work, by using FVDA, we find
 621 a clear delay of > 500 seconds between the release time of in-situ electrons and the re-
 622 lease time of 12–25 and 25–50 keV HXRs. Our work shows that for comparative stud-
 623 ies between in-situ electrons and HXRs, it is important to use the FVDA to obtain ac-
 624 curate estimates of electron release times at the Sun.

625 We use 1-minute as the threshold for determining if the release of in-situ electrons
 626 is energy-dependent or energy-independent. One relevant question one can ask is how
 627 much does the result depend on this choice of threshold? If we relax this threshold to
 628 2 minutes, as shown in Figure 4, we find that events 2, 4, and 26 will also become energy-
 629 independent release events. However, event 2 only has data from four energy channels,
 630 and the release times for these four energy channels show a monotonous increase with
 631 electron energy. If this energy dependence continues to a higher energy channel, then
 632 the release time difference between this energy channel and the lowest energy channel
 633 can exceed 2 minutes. So event 2 may or may not be classified as an energy-independent
 634 release event. For event 4, the path length from Approach I is 1.32 ± 0.04 au. This is
 635 to be compared with the Parker field path length of 1.11 au in Approach II. The differ-
 636 ence, 0.21 au, is larger than those in events 3, 5 and 8. Nevertheless, when relaxing the
 637 threshold to 2 minutes, the release time differences for both a path length of 1.11 and
 638 1.32 au are within 2 minutes, making event 4 an energy-independent release event. For
 639 event 26, the path length from Approach I is 0.99 ± 0.02 au, consistent with 1.0 au, and
 640 the Parker path length is 1.10 au. Relaxing the threshold to 2.0 minutes, release time
 641 differences from both Approach I and II in event 26 are also within the threshold (2 min-

642 utes). So Event 26 also becomes an energy-independent release event. In summary, when
 643 increasing the threshold to 2 minutes, a total of 5 events can be classified as energy-independent
 644 release events. We remark that the choice of the threshold should be larger than but close
 645 to the uncertainty of the release times. The FVDA method provides a measure of the
 646 uncertainty of the release time. As we discussed earlier, this uncertainty contains an in-
 647 trinsic 30-second uncertainty from the time resolution of in-situ electron data and ap-
 648 plying the Savitzky-Golay filter; as well as a fitting uncertainty that is often ~ 20 sec-
 649 onds. Therefore our choice of a 1-minute threshold is appropriate.

650 4 Conclusions

651 In this article, we perform a statistical study of the release time for 29 impulsive
 652 solar energetic electron events from 2002 to 2016 using in-situ electron data from Wind/3DP
 653 and hard X-ray observation from RHESSI and Fermi/GBM. Based on the recently de-
 654 veloped FVDA (Zhao et al., 2019), we examined the release time of both the outward-
 655 and downward-propagating near-relativistic electrons, and showed that for all events, there
 656 is a distinct time delay, mainly distributed between 0–1000 s, which is consistent with
 657 the case study of G. Li, Zhao, et al. (2020); G. Li et al. (2021). The release time of in-
 658 situ electrons also shows clear energy dependence with higher energy electrons released
 659 later, consistent with a time-dependent acceleration process. For 28 events where type
 660 III radio bursts are available, we also compare the release time of type III radio bursts
 661 and the release times of in-situ electrons. In 15 events, the timing of type III radio bursts
 662 is consistent with that of low-energy electrons. In 11 (2) events, the timing of type III
 663 radio bursts is earlier (later) than the release of in-situ electrons. In 7 out of these 11
 664 events, the timing of type III radio bursts is consistent with the HXR. Our results sug-
 665 gest that a delayed release of in-situ electrons compared to HXR is a common phenomenon
 666 and the HXR-generating electrons and the in-situ electrons are likely of two different pop-
 667 ulations in a majority of the events we examined. This finding is consistent with the sce-
 668 nario where electrons can be accelerated at both the outward and downward propagat-
 669 ing exhaust as proposed by Liu et al. (2013). Using a threshold of 1 minute, 26 of the
 670 29 events (i.e. $\sim 90\%$) show clear energy-dependent release for outward propagating elec-
 671 trons; in only one of these event (event 22), we find that high energy electrons are re-
 672 leased earlier than low energy electrons and in the other 25 events high energy electrons
 673 are released later than low energy electrons; in events 3, 5 and 8, i.e., 3 of the 29 events
 674 ($\sim 10\%$), electrons of different energies are released within 1 minute, showing no energy
 675 dependence. If we relax the duration threshold from 1 minute to 2 minutes, then events
 676 4 and 26 now become energy-independent release events, making the total number of energy-
 677 independent release events to 5. In the 26 events that show energy-dependent release,
 678 15 have electrons from 5 or more energy channels. For these events we extend the anal-
 679 ysis of G. Li et al. (2021) and fit the release time as a function of electron momentum
 680 by a power law as given by equation (5). The fitting parameter γ mainly distributed be-
 681 tween -3.5 to -2 , which correspond to a turbulence spectrum $\sim k^{-6.5}$ to k^{-5} at the
 682 acceleration site. Such a spectrum may indicate a dissipation range. The value of γ shows
 683 no correlation with the flare class and the delay in electron release time.

684 One result from this study is the identification of three events (3, 5, and 8) in which
 685 in-situ electrons are released simultaneously at the Sun but later than HXR-generating
 686 electrons. These are events that satisfy the implicit assumption of the VDA. However,
 687 the occurrence rate of these events is low, only $\sim 10\%$. The reason for this low frequency
 688 remains to be investigated.

689 One of the assumptions of the FVDA is the scatter-free assumption. This is a rea-
 690 sonable assumption if the electron path length is shorter than the electron mean free path.
 691 However, for events where electron's mean free path is comparable to the path length,
 692 the effect of scattering is important and has to be considered. In a recent work, Dröge
 693 et al. (2018) examined the 2002 October 20 event using a numerical approach which took

pitch angle scattering of electrons into account. The pitch angle scattering diffusion coefficient $D_{\mu\mu}$ has both radial and energy dependence. By working with level zero data from Wind/3DP and by comparing simulation with the observation, they suggested that a scatter-free assumption tends to work better for low-energy electrons than high-energy electrons. In another study, Tan et al. (2011) discussed the cause of the scatter-free transport of non-relativistic solar electrons. They examined the energy dependence of electron angular distributions and related it with the steepening of interplanetary magnetic field (IMF) power spectral densities, concluding that the scattering of energetic electrons (and protons) is energy-dependent. These studies signify the importance of the role of numerical simulation in understanding in-situ electron observations. It also implies that if we can observe impulsive events from a much closer distance than 1 au, then the propagation effect can be minimized. Recently, two heliospheric missions, namely Parker Solar Probe (PSP) and Solar Orbiter (SolO) have made considerable progress in observing SEP events. Observing the Sun from as close as $10R_s$ (PSP) and off the ecliptic plane (SolO), they are expected to see many more events with higher fluence and more details. Applying the FVDA method to these events will therefore have lower timing uncertainties than to events at 1 au. This will help us to learn more about the underlying particle acceleration and release process. Together with observations at 1 au, we may even have the opportunity to observe the same event from multiple spacecraft. Such a rare opportunity will help us to better understand the role of transport (pitch angle scattering) and to better decipher the energy dependence of the release time delay. As mentioned in section 3.3, we suggest a possible scenario in which the flare-driven reconnection between closed loops serve as a trigger of interchange reconnection, and an energy-independent release event can only be observed if the interchange reconnection is successfully induced and the open field line is well connected to the Earth. In these events, the observed delay between in-situ electrons and the downward-propagating electrons is possible if the in-situ electrons do not correspond to the first episode of HXR. Since the time profiles of HXR represent spatially-integrated solar atmosphere response to the precipitating electrons, the first episode of HXR represents the earliest precipitating electrons. Since the interchange reconnection does not occur at the very beginning of a flare, the release time of in-situ electrons is thus delayed from the onset time of the first HXR episode.

In a recent paper, W. Wang et al. (2021) examined the spectral relationship between HXR-producing electrons and SEEs and also concluded that the HXR-producing electrons and SEE electrons are of two different populations. They also suggested that two (or more) reconnection processes may occur at the reconnection site, and the HXR-generating electrons are electrons that experience two consecutive accelerations, i.e., they are downward-traveling electrons produced at the first reconnection site which occur high in the corona. Such a two-stage acceleration is consistent with our current study. Note that W. Wang et al. (2021) suggested that the HXR-generating electrons may occur after low energy (< 30 keV) outward SEEs. However, if the acceleration at the first reconnection site is not powerful, then outward propagating SEEs would also need to experience a secondary acceleration, therefore lag behind the HXR, as found in this paper. To further understand the electron acceleration process at a flare, the energy-independent release events, although rare, may yield valuable clues. Detailed studies of these events will be reported in the future.

5 Open Research

All data used in this work are publicly available at the CDAWeb database (<https://cdaweb.gsfc.nasa.gov/index.html/>). All event analysis data presented in the paper are archived in a dataset on Zenodo. The doi is <https://doi.org/10.5281/zenodo.7410328>.

Acknowledgments

Acknowledgments: XYW and SY are supported by a NSFC grant under contract No.42074204. GL acknowledges an UAH PI support. LW is supported in part by NSFC under contracts 42127803 and 42150105, in part by the China National Space Administration project (D020301). GL, SY, LW, FE also acknowledge supports from the ISSI team 469. Constructive suggestions from both referees are greatly appreciated.

References

- Anderson, K. A., Sommers, J., Lin, R. P., Pick, M., Chaizy, P., Murphy, N., ... Phillips, J. L. (1995). Mirroring of fast solar flare electrons on a downstream corotating interaction region. *Journal of Geophysical Research: Space Physics*, *100*(A1), 3-11. Retrieved from <https://agupubs.onlinelibrary.wiley.com/doi/abs/10.1029/94JA01811> doi: <https://doi.org/10.1029/94JA01811>
- Baba, K., Bahi, L., & Ouadif, L. (2014, October). Enhancing Geophysical Signals Through the Use of Savitzky-Golay filtering method. *Geofisica Internacional*, *53*(4), 399-409. Retrieved 2022-12-01, from <https://www.sciencedirect.com/science/article/pii/S0016716914700741> doi: 10.1016/S0016-7169(14)70074-1
- Battaglia, M., Sharma, R., Luo, Y., Chen, B., Yu, S., & Krucker, S. (2021, November). Multiple Electron Acceleration Instances during a Series of Solar Microflares Observed Simultaneously at X-Rays and Microwaves. *The Astrophysical Journal*, *922*(2), 134. Retrieved 2023-02-06, from <https://dx.doi.org/10.3847/1538-4357/ac2aa6> doi: 10.3847/1538-4357/ac2aa6
- Bian, N. H., & Li, G. (2022, January). Transport of Solar Energetic Particles along Stochastic Parker Spirals. *The Astrophysical Journal*, *924*(2), 120. Retrieved 2022-05-28, from <https://iopscience.iop.org/article/10.3847/1538-4357/ac2fab> doi: 10.3847/1538-4357/ac2fab
- Cairns, I. H., Lobzin, V. V., Donea, A., Tingay, S. J., McCauley, P. I., Oberoi, D., ... Williams, C. L. (2018). Low Altitude Solar Magnetic Reconnection, Type III Solar Radio Bursts, and X-ray Emissions. *Scientific Reports*, *8*, 1676. doi: 10.1038/s41598-018-19195-3
- Cane, H. V. (2003). Near-Relativistic Solar Electrons and Type III Radio Bursts. *The Astrophysical Journal*, *598*(2), 1403-1408. Retrieved from <http://stacks.iop.org/0004-637X/598/i=2/a=1403%7B%5C%25%7D5Cnhttp://iopscience.iop.org/0004-637X/598/2/1403> doi: 10.1086/379007
- Carmichael, H. (1964). *in Physics of Solar Flares*, 451.
- Dröge, W., Kartavykh, Y. Y., Wang, L., Telsoni, D., & Bruno, R. (2018). Transport Modeling of Interplanetary Electrons in the 2002 October 20 Solar Particle Event. *The Astrophysical Journal*, *869*(2), 168. Retrieved from <http://dx.doi.org/10.3847/1538-4357/aaec6c> doi: 10.3847/1538-4357/aaec6c
- Guo, L., Li, G., Reeves, K., & Raymond, J. (2017, September). Solar Flare Termination Shock and Synthetic Emission Line Profiles of the Fe xxi 1354.08 Line. *The Astrophysical Journal*, *846*, L12. Retrieved 2021-09-28, from <https://ui.adsabs.harvard.edu/abs/2017TheAstrophysicalJournal...846L..12G> (ADS Bibcode: 2017The Astrophysical Journal...846L..12G) doi: 10.3847/2041-8213/aa866a
- Haggerty, D. K., & Roelof, E. C. (2002). Impulsive Near-relativistic Solar Electron Events: Delayed Injection with Respect to Solar Electromagnetic Emission. *The Astrophysical Journal*, *579*(2), 841-853. (Number: 2) doi: 10.1086/342870
- Haggerty, D. K., Roelof, E. C., & Simnett, G. M. (2003). Escaping near-relativistic electron beams from the solar corona. *Advances in Space Research*, *32*(12), 2673-2678. (Number: 12) doi: 10.1016/S0273-1177(03)00929-3

- 797 Heyvaerts, J., Priest, E. R., & Rust, D. M. (1977). An emerging flux model for the
798 solar phenomenon. *The Astrophysical Journal*, *216*, 123–137. doi: 10.1086/
799 155453
- 800 Hirayama, T. (1974). Theoretical Model of Flares and Prominences. I: Evaporating
801 Flare Model. *solphys*, *34*(2), 323–338. (Number: 2) doi: 10.1007/BF00153671
- 802 Jokipii, J. R. (1966). Cosmic-Ray Propagation. I. Charged Particles in a Random
803 Magnetic Field. *The Astrophysical Journal*, *146*, 480. doi: 10.1086/148912
- 804 Klein, K.-L., Krucker, S., Trotter, G., & Hoang, S. (2005, March). Coronal phe-
805 nomena at the release of solar energetic electron events. *Astronomy & Astro-*
806 *physics*, *431*(3), 1047–1060. Retrieved 2022-04-12, from [http://www.aanda](http://www.aanda.org/10.1051/0004-6361:20041258)
807 [.org/10.1051/0004-6361:20041258](http://www.aanda.org/10.1051/0004-6361:20041258) doi: 10.1051/0004-6361:20041258
- 808 Kopp, R. A., & Pneuman, G. W. (1976). Magnetic reconnection in the corona and
809 the loop prominence phenomenon. *solphys*, *50*(1), 85–98. (Number: 1) doi:
810 10.1007/BF00206193
- 811 Krucker, S., Kontar, E. P., Christe, S., & Lin, R. P. (2007, July). Solar Flare
812 Electron Spectra at the Sun and near the Earth. *The Astrophysical Journal*,
813 *663*(2), L109–L112. Retrieved 2020-07-17, from [https://iopscience.iop](https://iopscience.iop.org/article/10.1086/519373)
814 [.org/article/10.1086/519373](https://iopscience.iop.org/article/10.1086/519373) (Number: 2) doi: 10.1086/519373
- 815 Krucker, S., Larson, D. E., Lin, R. P., & Thompson, B. J. (1999, jul). On the ori-
816 gin of impulsive electron events observed at 1 AU. *The Astrophysical Journal*,
817 *519*(2), 864–875. Retrieved from <https://doi.org/10.1086/307415> doi: 10
818 .1086/307415
- 819 Laitinen, T., Huttunen-Heikinmaa, K., Valtonen, E., & Dalla, S. (2015). COR-
820 RECTING FOR INTERPLANETARY SCATTERING IN VELOCITY DIS-
821 PERSION ANALYSIS OF SOLAR ENERGETIC PARTICLES. *The Astro-*
822 *physical Journal*, *806*(1), 114. Retrieved 2022-05-20, from [https://doi.org/](https://doi.org/10.1088/0004-637x/806/1/114)
823 [10.1088/0004-637x/806/1/114](https://doi.org/10.1088/0004-637x/806/1/114) (Publisher: American Astronomical Society)
824 doi: 10.1088/0004-637X/806/1/114
- 825 Li, G., Kong, X., Zank, G., & Chen, Y. (2013). On the Spectral Hardening at
826 gsim300 keV in Solar Flares. *The Astrophysical Journal*, *769*(1), 22. (Number:
827 1 _eprint: 1303.5917) doi: 10.1088/0004-637X/769/1/22
- 828 Li, G., Wu, X., Effenberger, F., Zhao, L., Lesage, S., Bian, N., & Wang,
829 L. (2021). Constraints on the Electron Acceleration Process
830 in Solar Flare: A Case Study. *Geophysical Research Letters*,
831 *48*(20), e2021GL095138. Retrieved 2021-12-21, from [https://](https://onlinelibrary.wiley.com/doi/abs/10.1029/2021GL095138)
832 onlinelibrary.wiley.com/doi/abs/10.1029/2021GL095138 (_eprint:
833 <https://onlinelibrary.wiley.com/doi/pdf/10.1029/2021GL095138>) doi:
834 10.1029/2021GL095138
- 835 Li, G., Wu, X., Zhao, L., & Yao, S. (2020, December). Observations of Outward-
836 propagating and Mirroring of the Same Energetic Electrons by Wind. *The*
837 *Astrophysical Journal Letters*, *905*(1), L1. Retrieved 2021-12-21, from
838 <https://iopscience.iop.org/article/10.3847/2041-8213/abca87> doi:
839 10.3847/2041-8213/abca87
- 840 Li, G., Zhao, L., Wang, L., Liu, W., & Wu, X. (2020, September). Identification of
841 Two Distinct Electron Populations in an Impulsive Solar Energetic Electron
842 Event. *The Astrophysical Journal*, *900*(2), L16. Retrieved 2020-11-10, from
843 <https://iopscience.iop.org/article/10.3847/2041-8213/abb098> doi:
844 10.3847/2041-8213/abb098
- 845 Li, X., Guo, F., Li, H., & Li, G. (2017, July). Particle Acceleration during Mag-
846 netic Reconnection in a Low-beta Plasma. *The Astrophysical Journal*, *843*,
847 21. Retrieved 2021-09-17, from [https://ui.adsabs.harvard.edu/abs/](https://ui.adsabs.harvard.edu/abs/2017TheAstrophysicalJournal...843...21L)
848 [2017TheAstrophysicalJournal...843...21L](https://ui.adsabs.harvard.edu/abs/2017TheAstrophysicalJournal...843...21L) (ADS Bibcode: 2017The
849 Astrophysical Journal...843...21L) doi: 10.3847/1538-4357/aa745e
- 850 Li, Y., Xue, J. C., Ding, M. D., Cheng, X., Su, Y., Feng, L., ... Gan, W. Q. (2018).
851 Spectroscopic Observations of a Current Sheet in a Solar Flare. *The Astro-*

- 852 *physical Journal*, 853(1), L15. doi: 10.3847/2041-8213/aaa6c0
- 853 Lin, R. P. (1974). Non-Relativistic Solar Electrons. *Space Science Reviews*, 16,
- 854 189.
- 855 Lin, R. P. (1985). Energetic Solar Electrons in the Interplanetary Medium. *Solar*
- 856 *Physics*, 100, 537.
- 857 Lin, R. P., Anderson, K. A., Ashford, S., Carlson, C., Curtis, D., Ergun, R., ...
- 858 Paschmann, G. (1995, February). A three-dimensional plasma and energetic
- 859 particle investigation for the wind spacecraft. *Space Science Reviews*, 71(1),
- 860 125–153. Retrieved 2022-04-13, from <https://doi.org/10.1007/BF00751328>
- 861 doi: 10.1007/BF00751328
- 862 Lintunen, J., & Vainio, R. (2004, June). Solar energetic particle event onset as
- 863 analyzed from simulated data. *Astronomy & Astrophysics*, 420(1), 343–350.
- 864 Retrieved 2022-05-20, from [https://www.aanda.org/articles/aa/abs/](https://www.aanda.org/articles/aa/abs/2004/22/aa0247/aa0247.html)
- 865 [2004/22/aa0247/aa0247.html](https://www.aanda.org/articles/aa/abs/2004/22/aa0247/aa0247.html) (Number: 1 Publisher: EDP Sciences) doi:
- 866 10.1051/0004-6361:20034247
- 867 Liu, W., Chen, Q., & Petrosian, V. (2013). Plasmoid Ejections and Loop Con-
- 868 tractions in an Eruptive M7.7 Solar Flare: Evidence of Particle Acceleration
- 869 and Heating in Magnetic Reconnection Outflows. *The Astrophysical Journal*,
- 870 767(2), 168. (Number: 2 eprint: 1303.3321) doi: 10.1088/0004-637X/767/2/
- 871 168
- 872 Masson, S., Antiochos, S. K., & DeVore, C. R. (2013). A Model for the Escape of
- 873 Solar-flare-accelerated Particles. *The Astrophysical Journal*, 771(2), 82. (Num-
- 874 ber: 2 eprint: 1301.0654) doi: 10.1088/0004-637X/771/2/82
- 875 Meegan, C., Lichti, G., Bhat, P. N., Bissaldi, E., Briggs, M. S., Connaughton, V.,
- 876 ... Wilson-Hodge, C. (2009). The Fermi Gamma-ray Burst Monitor. *The*
- 877 *Astrophysical Journal*, 702(1), 791–804. (Number: 1 eprint: 0908.0450) doi:
- 878 10.1088/0004-637X/702/1/791
- 879 Mitchell, J. G., de Nolfo, G. A., Hill, M. E., Christian, E. R., McComas, D. J.,
- 880 Schwadron, N. A., ... Szalay, J. R. (2020, October). Small Electron Events
- 881 Observed by Parker Solar Probe/IS \odot IS during Encounter 2. *The Astrophys-*
- 882 *ical Journal*, 902(1), 20. Retrieved 2023-02-06, from [https://dx.doi.org/](https://dx.doi.org/10.3847/1538-4357/abb2a4)
- 883 [10.3847/1538-4357/abb2a4](https://dx.doi.org/10.3847/1538-4357/abb2a4) doi: 10.3847/1538-4357/abb2a4
- 884 Moradi, A., & Li, G. (2019). Propagation of Scatter-free Solar Energetic Electrons
- 885 in a Meandering Interplanetary Magnetic Field. *The Astrophysical Journal*,
- 886 887(1), 102. (Number: 1) doi: 10.3847/1538-4357/ab4f68
- 887 Savitzky, A., & Golay, M. J. E. (1964, July). Smoothing and Differentiation of Data
- 888 by Simplified Least Squares Procedures. *Analytical Chemistry*, 36(8), 1627–
- 889 1639. Retrieved 2020-05-05, from <https://doi.org/10.1021/ac60214a047>
- 890 (Publisher: American Chemical Society) doi: 10.1021/ac60214a047
- 891 Sharma, R., Battaglia, M., Luo, Y., Chen, B., & Yu, S. (2020, November). Ra-
- 892 dio and X-Ray Observations of Short-lived Episodes of Electron Acceleration
- 893 in a Solar Microflare. *The Astrophysical Journal*, 904(2), 94. Retrieved
- 894 2023-02-06, from <https://dx.doi.org/10.3847/1538-4357/abbd96> doi:
- 895 10.3847/1538-4357/abbd96
- 896 Simnett, G. M., Roelof, E. C., & Haggerty, D. K. (2002, November). The Ac-
- 897 celeration and Release of Near-relativistic Electrons by Coronal Mass Ejec-
- 898 tions. *The Astrophysical Journal*, 579(2), 854. Retrieved 2022-04-12, from
- 899 <https://iopscience.iop.org/article/10.1086/342871/meta> (Publisher:
- 900 IOP Publishing) doi: 10.1086/342871
- 901 Smith, D. M., Lin, R. P., Turin, P., Curtis, D. W., Primbsch, J. H., Campbell,
- 902 R. D., ... Schwartz, R. (2003). The RHESSI Spectrometer. In R. P. Lin,
- 903 B. R. Dennis, & A. O. Benz (Eds.), *The Reuven Ramaty High-Energy Solar*
- 904 *Spectroscopic Imager (RHESSI)* (pp. 33–60). Dordrecht: Springer Nether-
- 905 lands. Retrieved 2020-09-22, from [http://link.springer.com/10.1007/](http://link.springer.com/10.1007/978-94-017-3452-3_2)
- 906 [978-94-017-3452-3_2](http://link.springer.com/10.1007/978-94-017-3452-3_2) doi: 10.1007/978-94-017-3452-3_2

- 907 Sturrock, P. A. (1966). Model of the High-Energy Phase of Solar Flares. *nat*,
 908 *211*(5050), 695–697. (Number: 5050) doi: 10.1038/211695a0
- 909 Tan, L. C., Malandraki, O. E., Reames, D. V., Ng, C. K., Wang, L., & Dorrian,
 910 G. (2012, April). USE OF INCIDENT AND REFLECTED SOLAR
 911 PARTICLE BEAMS TO TRACE THE TOPOLOGY OF MAGNETIC
 912 CLOUDS. *The Astrophysical Journal*, *750*(2), 146. Retrieved 2022-11-18,
 913 from <https://dx.doi.org/10.1088/0004-637X/750/2/146> (Publisher: The
 914 American Astronomical Society) doi: 10.1088/0004-637X/750/2/146
- 915 Tan, L. C., Reames, D. V., Ng, C. K., Saloniemi, O., & Wang, L. (2009, Au-
 916 gust). OBSERVATIONAL EVIDENCE ON THE PRESENCE OF AN
 917 OUTER REFLECTING BOUNDARY IN SOLAR ENERGETIC PARTICLE
 918 EVENTS. *The Astrophysical Journal*, *701*(2), 1753. Retrieved 2022-12-02,
 919 from <https://dx.doi.org/10.1088/0004-637X/701/2/1753> (Publisher: The
 920 American Astronomical Society) doi: 10.1088/0004-637X/701/2/1753
- 921 Tan, L. C., Reames, D. V., Ng, C. K., Shao, X., & Wang, L. (2011). What causes
 922 scatter-free transport of non-relativistic solar electrons? *Astrophysical Journal*,
 923 *728*(2). doi: 10.1088/0004-637X/728/2/133
- 924 Vech, D., Mallet, A., Klein, K. G., & Kasper, J. C. (2018). Magnetic Reconnec-
 925 tion May Control the Ion-scale Spectral Break of Solar Wind Turbulence. *The*
 926 *Astrophysical Journal*, *855*(2), L27. Retrieved 2022-04-28, from [https://doi](https://doi.org/10.3847/2041-8213/aab351)
 927 [.org/10.3847/2041-8213/aab351](https://doi.org/10.3847/2041-8213/aab351) (Publisher: American Astronomical Soci-
 928 ety) doi: 10.3847/2041-8213/aab351
- 929 Vrnak, B., Warmuth, A., Marii, D., Otruba, W., & Rudjak, V. (2003). Inter-
 930 action of an Erupting Filament with the Ambient Magnetoplasma and Es-
 931 cape of Electron Beams. *solphys*, *217*(1), 187–198. (Number: 1) doi:
 932 10.1023/A:1027388929859
- 933 Wang, L., Krucker, S., Mason, G. M., Lin, R. P., & Li, G. (2016). The injection of
 934 ten electron/ 3 He-rich SEP events. *Astron. Astrophys.*, *585*, A119. Retrieved
 935 from <http://www.aanda.org/10.1051/0004-6361/201527270> doi: 10.1051/
 936 0004-6361/201527270
- 937 Wang, L., Lin, R. P., & Krucker, S. (2011). Pitch-angle Distributions and Tempo-
 938 ral Variations of 0.3-300 keV Solar Impulsive Electron Events. *The Astrophysi-
 939 cal Journal*, *727*(2), 121. (Number: 2) doi: 10.1088/0004-637X/727/2/121
- 940 Wang, L., Lin, R. P., Krucker, S., & Gosling, J. T. (2006). Evidence for double
 941 injections in scatter-free solar impulsive electron events. *Geophys. Res. Lett.*,
 942 *33*(3), 1–5. (Number: 3) doi: 10.1029/2005GL024434
- 943 Wang, L., Lin, R. P., Krucker, S., & Mason, G. M. (2012, October). A STATIS-
 944 TICAL STUDY OF SOLAR ELECTRON EVENTS OVER ONE SOLAR
 945 CYCLE. *The Astrophysical Journal*, *759*(1), 69. Retrieved 2020-04-06, from
 946 <https://doi.org/10.1088/0004-637X/759/1/69> (Publisher: IOP
 947 Publishing) doi: 10.1088/0004-637X/759/1/69
- 948 Wang, W., Wang, L., Krucker, S., Mason, G. M., Su, Y., & Bučík, R. (2021). Solar
 949 Energetic Electron Events Associated with Hard X-Ray Flares. *The Astrophys-
 950 ical Journal*, *913*(2), 89. doi: 10.3847/1538-4357/abefce
- 951 Williams, P. E., & Pesnell, W. D. (2011, January). Properties of Supergran-
 952 ulation During the Solar Minima of Cycles 22/23 and 23/24. *Journal*
 953 *of Physics: Conference Series*, *271*(1), 012082. Retrieved 2023-02-06,
 954 from <https://dx.doi.org/10.1088/1742-6596/271/1/012082> doi:
 955 10.1088/1742-6596/271/1/012082
- 956 Zhao, L., Li, G., Zhang, M., Wang, L., Moradi, A., & Effenberger, F. (2019, June).
 957 Statistical Analysis of Interplanetary Magnetic Field Path Lengths from Solar
 958 Energetic Electron Events Observed by WIND. *The Astrophysical Journal*,
 959 *878*(2), 107. Retrieved 2020-04-06, from [https://iopscience.iop.org/
 960 article/10.3847/1538-4357/ab2041](https://iopscience.iop.org/article/10.3847/1538-4357/ab2041) doi: 10.3847/1538-4357/ab2041